RSC Advances

PAPER

View Article Online
View Journal | View Issue

Cite this: *RSC Adv.*, 2025, **15**, 6015

Utility of 6-aza-2-thiothymine in the synthesis of novel [1,2,4]triazolo[4,3-*b*][1,2,4]triazin-7-one derivatives: synthesis, structure elucidation, molecular docking and *in vitro* anti-lung cancer activity†

Monica G. Kamel,[a] Farid M. Sroor,[*b] Khaled Mahmoud,[c] Heba I. Shafey,[d] Hamdi M. Hassaneen[*a] and Laure Vendier[e]

Using 6-aza-2-thiothymine (ATT) as a suitable precursor, a novel series of [1,2,4]triazolo[4,3-*b*][1,2,4]triazin-7-one derivatives (**7a–j**) was prepared by refluxing 6-methyl-3-thioxo-3,4-dihydro-1,2,4-triazin-5(2*H*)-one (**3**) with hydrazonoyl halides (**1a–j**) in chloroform in the presence of triethylamine. The structures of the newly synthesized compounds **7a–j** were confirmed using spectral data, elemental analyses, and single-crystal X-ray diffraction results. All the synthesized triazolotriazin-7-one derivatives (**7a–j**) were evaluated as *in vitro* anti-cancer agents against PC3 (prostate cell line), A549 (lung carcinoma), PACA2 (pancreatic cancer cell line) and BJ1 (normal skin fibroblast) cell lines using MTT assay. Compounds **7a** and **7g** showed greater efficacy and low IC_{50} values (36.6 and 40.1 μM, respectively) compared to the reference drug, which exhibited an IC_{50} value of 43.8 μM on the lung cell line, and demonstrated safe mortality effect on the normal cell line (BJ1) with cytotoxicity percentages of 3.5% and 2.8%, respectively. These compounds (**7a** and **7g**) were the most active compounds of the synthesized triazolotriazin-7-one derivatives (**7a–j**). They were further investigated to ascertain their mechanism of action using DNA fragmentation, DNA damage and gene expression (BCL-2, BAX, and p53 genes). Results indicated a significant increase in the expression levels of BCL-2 and a reduction in the expression of p53 and BAX genes in negative lung cancer cell lines. However, the treatment of negative cell lines with **7g** improved the expression of the tested genes to a greater extent than that with **7a**. Additionally, the DNA damage and DNA fragmentation levels were significantly elevated in the lung cancer cell line samples treated with **7a** much more than **7g**. Molecular docking was employed to explore the potential interactions between the most active compounds (**7a** and **7g**) and two key enzymes, human 3-phosphoglycerate dehydrogenase (PHGDH) and phosphoserine aminotransferase (PSAT1), which play vital roles in the progression of lung cancer.

Received 22nd December 2024
Accepted 8th February 2025

DOI: 10.1039/d4ra08958h

rsc.li/rsc-advances

Introduction

Triazolotriazine moiety has attracted significant interest in medicinal chemistry owing to its unusual structural and electrical characteristics, which improve the efficacy of therapeutic candidates.[1–4] Its core is useful in the development of nucleoside analogs and other therapeutic medicines because it shows enhanced lipophilicity and improved binding interactions with biological targets.[1,5] Its incorporation in potential drug candidates has been demonstrated to improve antiviral and anticancer properties, mainly by increasing the drug's potency and selectivity against particular enzymes and receptors.[6,7] Furthermore, triazolotriazine moiety can improve the pharmacokinetic profiles of drugs and stabilize nucleic acid structures, enhancing bioavailability and lowering toxicity, respectively.[7,8] The significance of triazolotriazine derivatives in the synthesis of novel therapeutic agents highlights their potential for treating a range of diseases, such as cancer and viral infections.

Lung cancer continues to be one of the most widespread and lethal types of cancer worldwide, causing serious problems to public health.[9,10] Often discovered at an advanced stage, this

[a]*Department of Chemistry, Faculty of Science, Cairo University, Giza, Egypt. E-mail: hamdi_251@yahoo.com; hhassaneen@sci.cu.edu.eg*

[b]*Organometallic and Organometalloid Chemistry Department, National Research Centre, 12622 Cairo, Egypt. E-mail: faridsroor@gmx.de; fm.sroor@nrc.sci.eg*

[c]*Pharmacognosy Department, Pharmaceutical and Drug Industry Institute, National Research Centre, 12622-Dokki, Egypt*

[d]*Cell Biology Department, National Research Centre, 12622-Dokki, Egypt*

[e]*LCC-CNRS, Université de Toulouse, CNRS, UPS, Toulouse, France*

† Electronic supplementary information (ESI) available. CCDC 2390251. For ESI and crystallographic data in CIF or other electronic format see DOI: https://doi.org/10.1039/d4ra08958h

disease is characterized by the uncontrolled proliferation of aberrant cells in the lungs, which results in poor prognosis and limited therapeutic options.[11] The majority of lung cancer cases are caused by smoking, which is one of the main causes of the disease; however, risk factors for non-smokers include genetic predisposition, radon exposure, and environmental pollution.[12] Moreover, the heterogeneity of lung cancer, which results in different subtypes displaying unique molecular profiles, makes treatment plans more challenging to implement and calls for personalized approaches.[13] Targeted therapy and immunotherapy have made significant advances in lung cancer. However, issues including drug resistance, treatment expenses, and the necessity for early diagnostic technologies make it difficult to manage patients effectively and increase survival rates.[14,15] Addressing these challenges requires an integrated strategy that includes prevention, early diagnosis, and the development of innovative therapeutic strategies, including discovering new drugs to improve the outcomes for patients with lung cancer.

Given the above information, the purpose of this study was to design and synthesize novel triazolo[4,3-*b*][1,2,4]triazin-7-one derivatives (**7a–j**) as the triazolotriazine family using 6-aza-2-thiothymine (ATT) as a suitable precursor and evaluate their anti-cancer activity against various cancer cell lines, including the PC3 (Prostate cell line), A549 (Lung carcinoma), PACA2 (Pancreatic cancer cell line) and BJ1 (normal skin fibroblast). The synthesis of the triazolo[4,3-*b*][1,2,4]triazin-7-one derivatives was of special interest since these compounds were not investigated in previous studies. The most promising compounds (**7a** and **7g**) were examined in further studies to determine their mechanism of action using DNA fragmentation, DNA damage and gene expression (BCL-2, BAX, and p53 genes) as well as molecular docking.

Results and discussion

Chemistry

The reaction of 6-methyl-3-thioxo-3,4-dihydro-1,2,4-triazin-5(2*H*)-one (**3**)[16] with hydrazonoyl halides (**1a–j**) in refluxing chloroform in the presence of triethylamine yielded a single product in each case (**7a–j**), as shown in Scheme 1 and Fig. 1. In order to clarify the preceding results, Scheme 2 proposes two plausible mechanistic sequences. In the first sequence (route A in Scheme 2), nitrilimines (**2**), which are generated *in situ* by the base-catalyzed dehydrohalogenation of hydrazonoyl halides (**1**),[17–21] are thought to undergo 1,3-dipolar cycloaddition with the C=S double bond of triazinethione (**3**), resulting in the spiro intermediate **4**, which is then subjected to a base-catalyzed ring cleavage to yield thiohydrazide (**5**). Subsequent intramolecular cyclization of **5** may result in two distinct

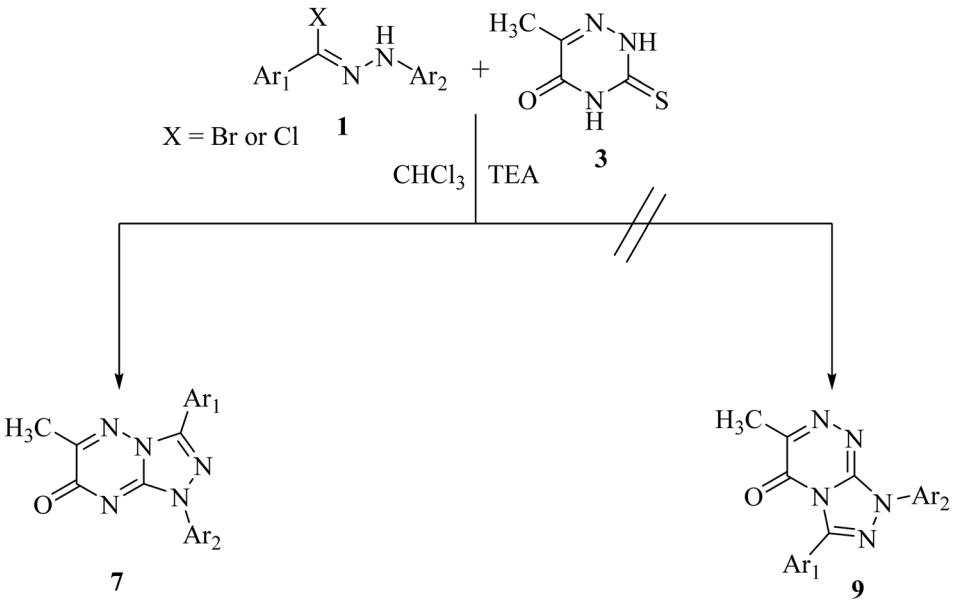

	Ar_1/Ar_2		Ar_1/Ar_2
a	$CH_3/4\text{-}NO_2C_6H_4$	**f**	$4\text{-}CH_3C_6H_4/C_6H_5$
b	$CH_3CH_2/4\text{-}NO_2C_6H_4$	**g**	$4\text{-}OCH_3C_6H_4/C_6H_5$
c	$CH_3CH_2CH_2/4\text{-}NO_2C_6H_4$	**h**	$4\text{-}ClC_6H_4/C_6H_5$
d	$(CH_3)_2CH/4\text{-}NO_2C_6H_4$	**i**	2-Furyl/$4\text{-}NO_2C_6H_4$
e	$(CH_3)_2CHCH_2/4\text{-}NO_2C_6H_4$	**j**	2-Thienyl/$4\text{-}NO_2C_6H_4$

Scheme 1 Synthesis of [1,2,4]triazolo[4,3-*b*][1,2,4]triazin-7-one derivatives **7a–j**.

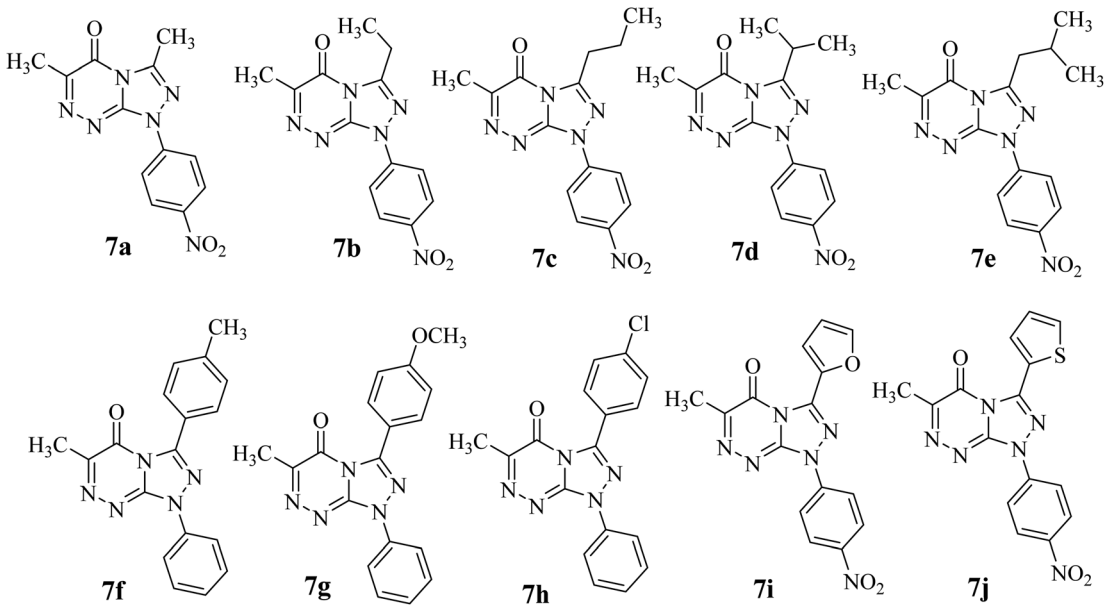

Fig. 1 Chemical structures of all the synthesized [1,2,4]triazolo[4,3-*b*][1,2,4]triazin-7-one derivatives (**7a–j**).

heterocyclic intermediates, **6** and **8**, which quickly lose hydrogen sulfide to form triazolo[4,3-*b*][1,2,4]triazin-7-one (**7**) or triazolo[3,4-*c*][1,2,4]triazin-5-one (**9**), respectively. In the intermediate **5**, the less nucleophilic nitrogen (N-4) could lead to a preferential ring closure to form [1,2,4]triazolo[4,3-*b*][1,2,4] triazin-7-one (**7**) owing to the electronic effect of the carbonyl group.[22] As an alternative, the reaction could include primary 1,3-addition, which results in amidrazones (**10**) that cyclize to give intermediate **11** and then compound **7** by the loss of hydrogen sulfide, as shown in route B in Scheme 2. It is suggested that route A is more likely to occur considering the following factors: (1) a C═S double bond appears to be a more reactive dipolarophile toward different 1,3-dipoles, (2) amidrazones of type **10** are known to be stable, but despite this, every attempt to separate them from the reaction mixtures was unsuccessful; (3) triazine-3-thione derivatives are mainly found in thione structures.[23]

The structures of the isolated products were identified by their elemental analyses and spectroscopic data (^{1}H NMR and ^{13}C NMR). Their structures were assigned to be **7** rather than the isomeric structure **9** (Scheme 1 and Fig. 1). For example, the ^{1}H NMR spectrum of compound **7b** showed the following signals: triplet at δ 1.48 corresponding to the methyl protons in $CH_2C\underline{H}_3$, singlet at δ 2.45 corresponding to CH_3 group protons, quartet at δ 3.03 corresponding to the methylene protons in $C\underline{H}_2CH_3$ and pair of doublets at δ 8.30 and 8.45 corresponding to the protons of 4-$NO_2C_6H_4$. Also, its ^{13}C NMR spectrum showed 11 signals for asymmetric carbon atoms. Moreover, the single crystal X-ray structure of **7b** confirmed the formation of a [1,2,4]triazolo [4,3-*b*][1,2,4]triazin-7-one scaffold (Table 1 and Fig. 2).

As depicted in Table 1 and Fig. 2, single crystals containing **7b** were found to be suitable for single-crystal X-ray diffraction. The crystal structure of compound **7b** was deposited at Cambridge Crystallographic Data Centre under CCDC number 2390251. It was produced as orange crystals from a saturated DMF/acetonitrile solution at ambient temperature. Compound **7b** forms a single molecule in the unit cell and crystallizes in the monoclinic cell with space group $P2_1/n$ (Table 1). The presence of the fused [1,2,4] triazolo[4,3-*b*][1,2,4]triazin-7-one scaffold was clearly elucidated by the crystal structure determination of 3-ethyl-6-methyl-1-(4-nitrophenyl)-[1,2,4]triazolo[4,3-*b*][1,2,4]triazin-7(1*H*)-one (**7b**) (Fig. 2). The selected examples of the bond lengths and angles of the [1,2,4] triazolo[4,3-*b*][1,2,4]triazin-7-one moiety, the distances of N7–N6 is 1.3721(14), N9–N1 is 1.3969(14), N7–C2 is 1.3648(16), C2–N1 is 1.3634 (15), N3–C2 is 1.3119(16), and C10–N1 is 1.4156(15), and the angles C8–N9–N1 is 106.15(10), O17–N16–O18 is 123.50(11), and N6–N7–C8 is 126.81(11), are in good agreement with those reported for 5-(4-bromophenyl)-4,6-dichloro-7-(2,4-dichlorophenyl)-7*H*-pyrrolo[2,3-*d*]pyrimidine, 4-amino-7-nitro-[1,2,4]triazolo[5,1-*c*][1,2,4]triazine-3-carbonitrile and 4,6-dichloro-7-(2,4-dichlorophenyl)-5-(3,4-dimethoxyphenyl)-7*H*-pyrrolo[2,3-*d*]pyrimidine.[3,24,25] More selected bond lengths and angles are shown in Fig. 2 (see ESI†).

Anti-cancer activity

***In vitro* cytotoxicity using MTT assay.** Using specific human cancer cell lines, the anti-proliferative effectiveness of compounds **7a–j** was evaluated in an *in vitro* assay. The anticancer activity of these compounds (**7a–j**) on various cancer cell lines, including PC3 (Prostate cell line), A549 (Lung carcinoma), PACA2 (Pancreatic cancer cell line) and BJ1 (normal skin fibroblast), was investigated in this study using the 3-(4,5-dimethylthiazol-2-yl)-2,5-diphenyltetrazolium bromide (MTT) test. Doxorubicin (**Dox**) was the standard medication used as a positive control.

In the initial screening trial, a single dosage concentration of 100 μg ml^{-1} was applied for 48 hours. The cytotoxicity of the treated cells was determined by calculating the cell death

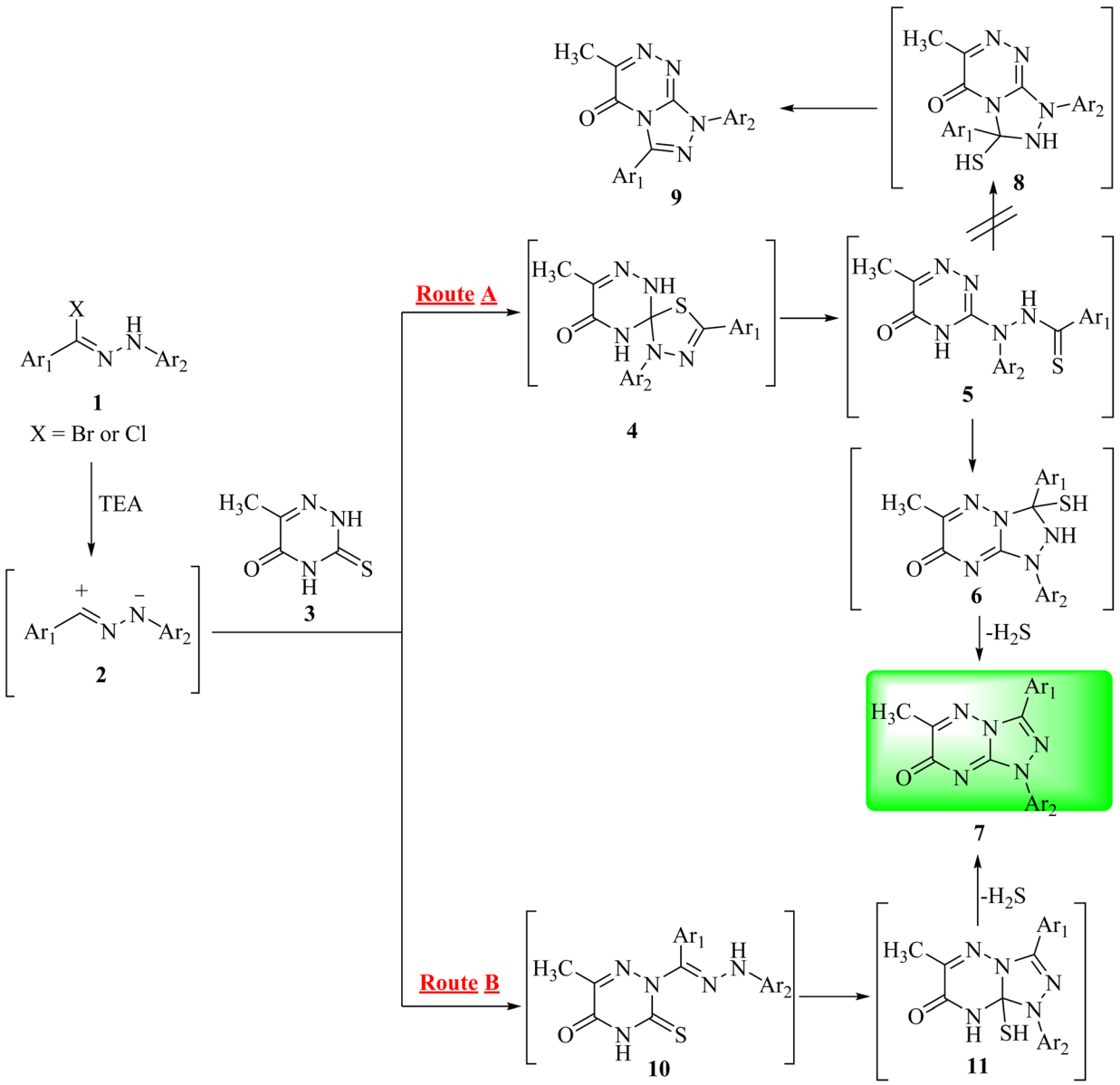

Scheme 2 Plausible mechanism of the synthesis of [1,2,4]triazolo[4,3-*b*][1,2,4]triazin-7-one derivatives (**7a–j**).

Table 1 Crystal structure data and details of the structure refinement for compound **7b**

CCDC deposition number	2390251	μ (Cu K$_\alpha$)/mm^{-1}	0.95
Chemical formula sum	$C_{13}H_{13}N_6O_3$	Crystal size/mm	0.19 × 0.18 × 0.14
Formula weight/g mol^{-1}	301.28	T/K	100
Crystal color and shape	Orange, Bloc	θ rang/°	4.2–79.4
Crystal system	Monoclinic	Reflections collected	2840
Space group	$P2_1/n$	λ (Å)	1.54184
Unit cell parameters			
a (Å)	8.0047 (3)	F000	628
b (Å)	21.1874 (6)	Extinction correction	None
c (Å)	8.0296 (3)	R_{Int}	0.042
α (°)	90	Parameters/restraints	203/4
β (°)	104.314 (4)	$R[F^2 > 2\sigma(F^2)]$	0.043
γ (°)	90	$wR(F^2)$	0.1294
Unit cell volume/Å^3	1319.53 (9)	Goodness-of-fit on F^2	0.9825
Molecules per cell Z	4	1-Sigma level	0.001
Calcd density ρ/g cm^{-3}	1.516	Highest difference peak and hole/e Å^{-3}	0.29/−0.64

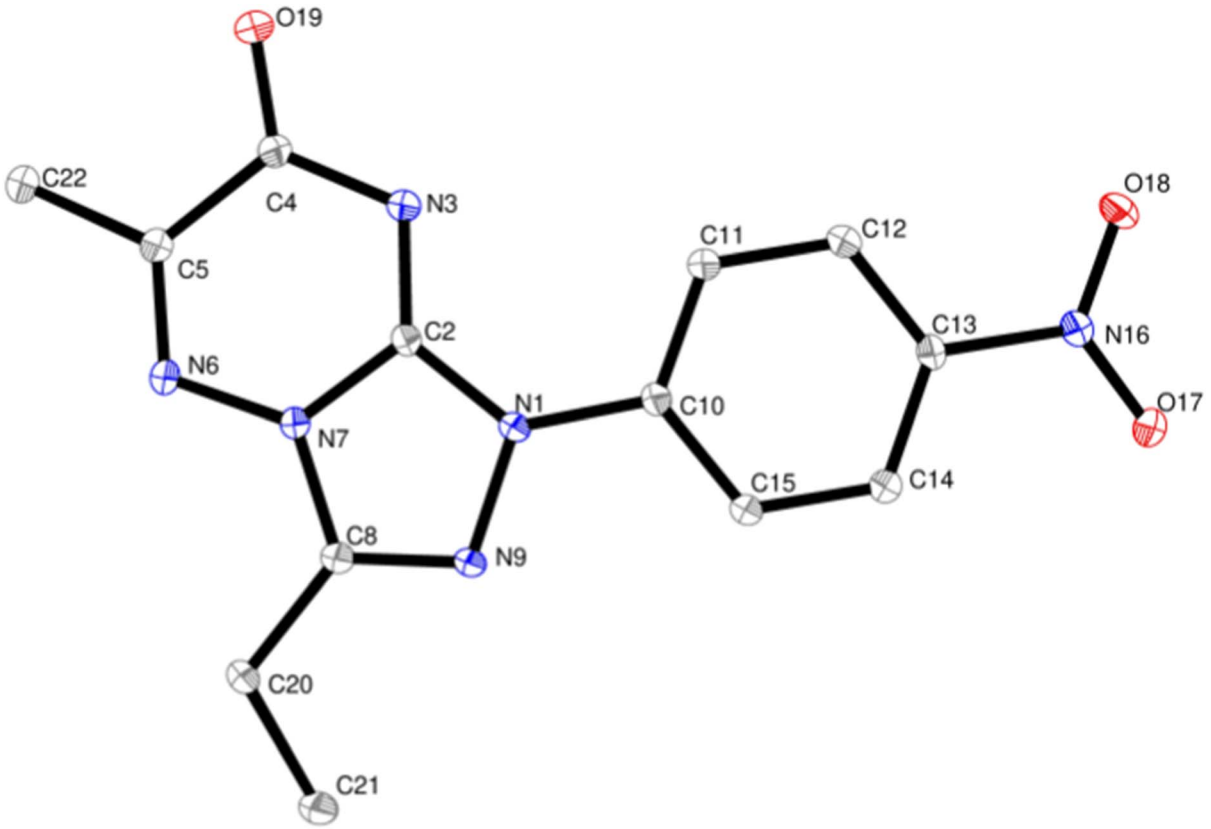

Fig. 2 Single-crystal structure of 3-ethyl-6-methyl-1-(4-nitrophenyl)-[1,2,4]triazolo[4,3-*b*][1,2,4]triazin-7(1*H*)-one (**7b**). H atoms are omitted for clarity. Selected bond lengths [Å]: N7–N6 1.3721(14), N9–N1 1.3969(14), N7–C2 1.3648(16), C2–N1 1.3634 (15), N3–C2 1.3119(16), C10–N1 1.4156(15), O19–C4 1.2236(16), C22–C5 1.4916(17), O17–N16 1.2289(15), O18–N16 1.2285(15). Selected bond angles [°]: C8–N9–N1 106.15(10), O17–N16–O18 123.50(11), N6–N7–C8 126.81(11), N6–N7–C2 123.68(11), C8–N7–C2 109.18(10), N9–N1–C2 110.77(10), N3–C2–N1 130.12(11).

percentage (% mortality) as a percentage of untreated cells (Table 2). Against the lung cancer cell lines (A549), the results demonstrated that four compounds, **7a**, **7e**, **7f** and **7g**, had considerable cytotoxic activity (80.4, 86.3, 69.1, and 82.3%, respectively), while compounds **7b**, **7d** and **7j** showed limited cytotoxic effects of 35.2, 33.3 and 32.8%, respectively (Table 2). In the case of the prostate cell line (PC3), all compounds showed limited anti-cancer activity with mortality in the range of 15.9–35.1%, as depicted in Table 2. All the synthesized triazolotriazin-7-one derivatives (**7a–j**) demonstrated a low cytotoxic effect on the pancreatic cancer cell line (PACA2), as shown in Table 2. Additionally, to confirm the safety of the most effective compounds against cancer cells, their cytotoxicity was assessed against normal cells (BJ1). As visualized in Table 1, the most promising compounds, **7a**, **7e**, **7f** and **7g**, were found to be safe on the normal cells (BJ1) up to a concentration of 100 μg

Table 2 (%) Mortality of cancer and normal cell lines at 100 μg ml^{-1} of compounds **7a–j** and IC_{50} (μM) values of the most active compounds

Compound	PC3 (IC_{50}, μM)	A549 (IC_{50}, μM)	PACA2 (IC_{50}, μM)	BJ1
7a	28.2 ± 0.25	80.4 ± 0.66 (**36.6 ± 0.33**)	20.4 ± 0.11	3.5 ± 1.16
7b	24.5 ± 0.57	35.2 ± 1.22	3.6 ± 0.21	4.2 ± 0.98
7c	27.3 ± 1.20	22.9 ± 0.81	10.5 ± 0.61	1.6 ± 0.38
7d	17.9 ± 0.38	33.3 ± 0.22	11.5 ± 0.25	36.2 ± 1.11
7e	35.1 ± 1.11	86.3 ± 0.74 (**42.5 ± 0.27**)	8.6 ± 0.33	6.4 ± 0.85
7f	33.4 ± 1.18	69.1 ± 0.77	5.6 ± 0.11	3.2 ± 0.63
7g	14.6 ± 0.92	82.3 ± 0.82 (**40.1 ± 0.84**)	13.4 ± 1.15	2.8 ± 0.71
7h	24.2 ± 0.21	13.5 ± 0.33	21.3 ± 0.98	9.6 ± 0.93
7i	18.4 ± 1.14	14.2 ± 0.24	9.6 ± 1.33	2.9 ± 1.22
7j	15.9 ± 0.51	32.8 ± 0.54	7.2 ± 0.88	3.8 ± 0.77
Dox	100 (**43.78 ± 0.54**)	100 (**43.80 ± 0.17**)	100 (**52.06 ± 0.42**)	1.10 ± 0.52
Negative control	0	0	0	0

ml^{-1} with cytotoxicity percentages 3.5%, 6.4%, 3.2%, and 2.8%, respectively.

Based on the results of Table 2, we continued our investigation into the molecular mechanisms underlying the potent lethal impact of the most active compounds on lung cancer cells (A549). Compounds **7a**, **7e**, **7f**, and **7g** showed limited mortality and high safety on the normal cells. Hence, secondary screening was performed on these compounds to ascertain their IC_{50} values and selectivity index. Table 2 illustrates that compounds **7a**, **7e**, and **7g** had greater efficacy (IC_{50} values of 36.6, 42.5, and 40.1 μM, respectively) in comparison to the reference drug with an IC_{50} of 43.8 μM. Accordingly, compounds **7a** and **7g** with low IC_{50} values (36.6 and 40.1 μM, respectively) and safe mortality effect on the normal cell line (BJ1) with cytotoxicity percentages of 3.5, and 2.8%, respectively, are the most active compounds of the synthesized triazolotriazin-7-one derivatives (**7a–j**). Thus, in order to explore the potential mode of action of compounds **7a** and **7g** as powerful anti-lung cancer agents, we selected them for further studies. We used comet, RT-PCR, and DNA fragmentation tests to examine the effects of these compounds at the gene, protein, and DNA levels.

Gene expression in lung cancer cell lines. The study of the expression of BCL-2, p53, and BAX in lung cancer cell lines treated with compounds **7a**, **7g**, and **Dox** is presented in Fig. 3–5. The results indicated a significant increase ($P < 0.01$) in the expression levels of the anti-apoptotic gene BCL-2 in negative samples of the lung cancer cell lines compared to the treated cell lines (Fig. 3).

Nonetheless, the expression levels of the pro-apoptotic genes (p53 and BAX) were dramatically diminished in the negative samples of lung cancer cell lines compared to the treated lung cancer cell lines (Fig. 4 and 5). The expression levels of the anti-apoptotic gene BCL-2 were diminished in descending order in the cancer cell lines treated with **7g**, **Dox**, and subsequently **7a** in comparison to the negative control cancer cell lines. The

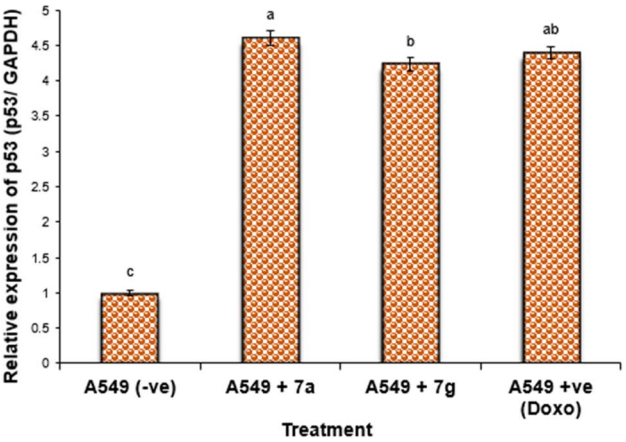

Fig. 4 Alterations in the p53 gene expression in lung cancer cell lines treated with **7a** and **7g** as well as **Dox**. Data are presented as mean ± SEM. [a, b, c]: Mean values within the tissue with unlike superscript letters were significantly different ($P < 0.05$).

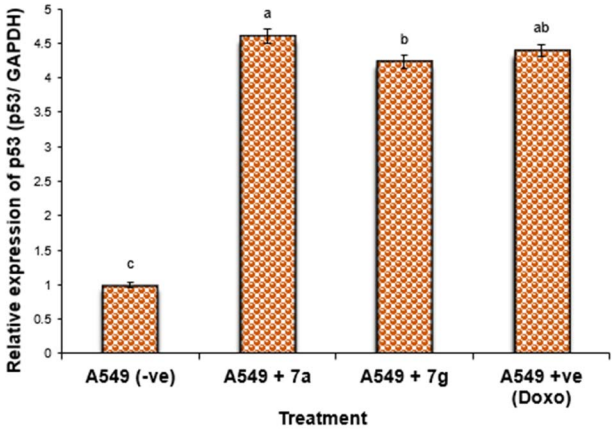

Fig. 5 Alterations in the BAX gene expression in lung cancer cell lines treated with **7a** and **7g** as well as **Dox**. Data are presented as mean ± SEM. [a, b, c]: Mean values within the tissue with unlike superscript letters were significantly different ($P < 0.05$).

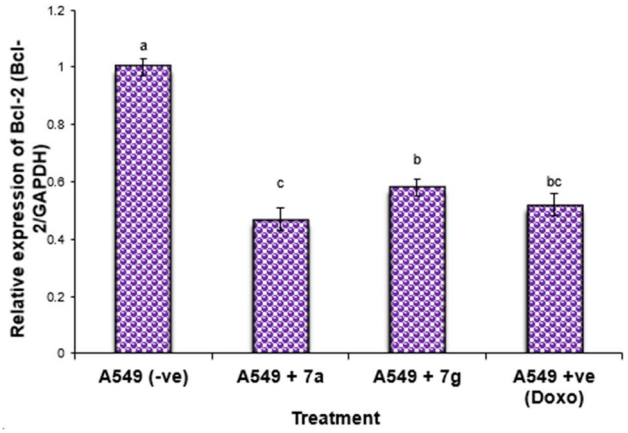

Fig. 3 Alterations in the BCL-2 gene expression in lung cancer cell lines treated with **7a** and **7g** as well as **Dox** (as positive control). Data are presented as mean ± SEM. [a, b, c]: Mean values within the tissue with unlike superscript letters were significantly different ($P < 0.05$).

expression levels of the pro-apoptotic genes (p53 and BAX) were elevated in a sequential manner in the cancer cell line treated with **7g**, followed by **Dox**, and subsequently **7a**, in comparison to the negative control cancer cell lines.

The results indicated that the anti-cancer action of the examined drugs was most prominently detected in **7g**, followed by **Dox**, and subsequently **7a**. Compound **7a** showed much greater efficacy against the tumor cell line compared to **7g**.

DNA damage evaluation using the comet assay. The DNA damage in lung cancer cell lines was assessed using the comet test, as illustrated in Table 3 and Fig. 6. The findings indicated that the negative lung cancer cell lines demonstrated a notable reduction ($P < 0.05$) in DNA damage values (11.59 ± 0.65). However, the DNA damage levels were significantly elevated ($P < 0.01$) in the lung cancer cell line samples treated with **7a** (28.181.25), **Dox** medication (23.861.11), and **7g** (21.140.85) in comparison to the negative control.

Table 3 Visual score of the DNA damage in lung cancer cell lines treated with **7a** and **7g**

Treatment	No. of samples	No. of cells		Class[b]				DNA damaged cells% (mean ± SEM)
		Analyzed[a]	Comets	0	1	2	3	
A549 (−ve)	4	440	51	389	35	12	4	11.59 ± 0.65[c]
A549 + **7a**	4	440	124	316	37	45	42	28.18 ± 1.25[a]
A549 + **7g**	4	440	93	347	32	38	23	21.14 ± 0.85[b]
A549 + **Dox**	4	440	105	335	34	41	30	23.86 ± 1.11[b]

[a] Number of cells examined per group. [b] Class 0 = no tail; 1 = tail length < diameter of the nucleus; 2 = tail length between 1× and 2× the diameter of the nucleus; and 3 = tail length > 2× the diameter of the nucleus.

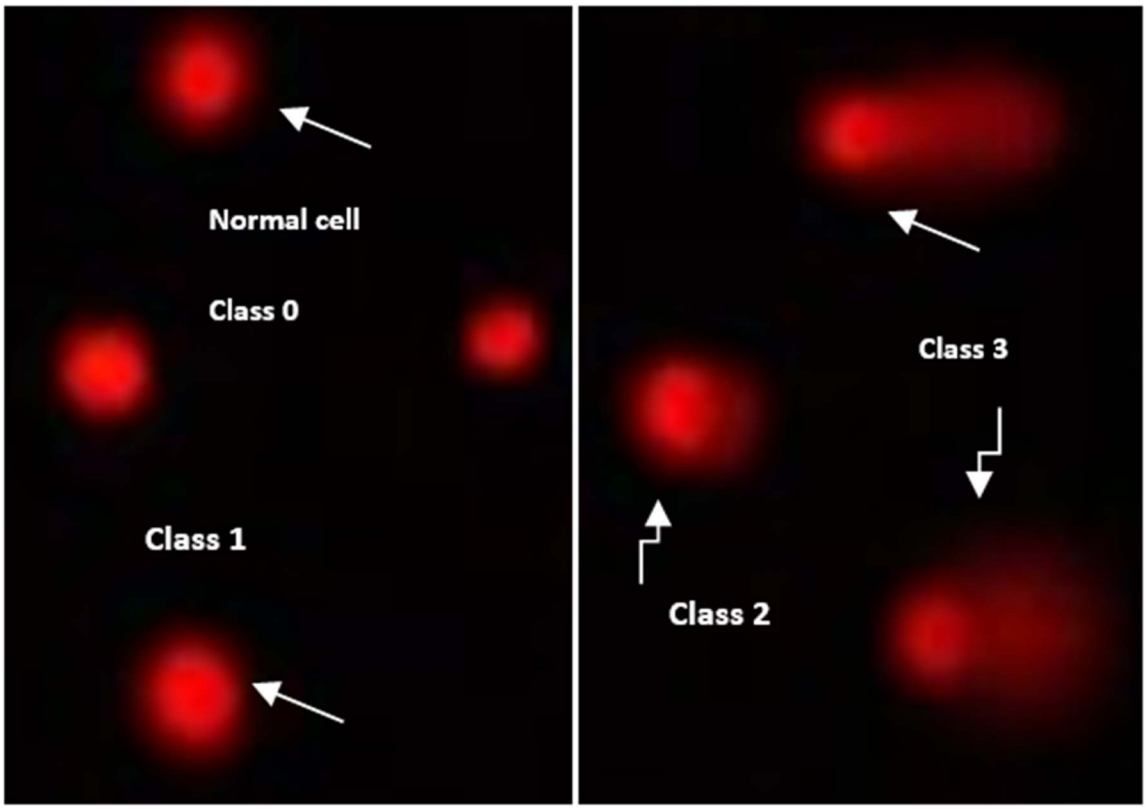

Fig. 6 Visual score of normal DNAs (class 0) and damaged DNAs (class 1, class 2 and class 3) using comet assay in lung cancer cell lines.

Measurement of DNA fragmentation in lung cancer cell lines. The DNA fragmentation evaluation of compounds **7a** and **7g** against the lung cancer cell is depicted in Fig. 7 and 8 as well as Table 4. However, the DNA fragmentation values increased significantly ($P < 0.01$) in the lung cancer cell line samples treated with **7a** (32.78 ± 1.35), doxorubicin (28.38 ± 1.06) and **7g** (25.57 ± 0.94) compared with the negative control cancer cell lines (12.54 ± 0.45) (Table 5).

Molecular docking. Molecular docking is a valuable computational technique for assessing the binding interaction between a ligand and the active site of an enzyme or receptor. In this study, molecular docking was employed to explore the potential interactions between the most active compounds (**7a** and **7g**) and two key enzymes, human 3-phosphoglycerate dehydrogenase (PHGDH) and phosphoserine aminotransferase (PSAT1), which play vital roles in the progression of lung cancer.

Autodock Vina within PyRx software version 8 was utilized to conduct the docking simulations, and the binding energy was used to report the results for each compound. A lower binding energy value signifies a stronger binding affinity. Hydrogen bonds, the strongest interactions, were examined in conjunction with hydrophobic bonds (carbon–hydrogen, van der Waals, Pi–anion, Pi–cation, Pi–sigma, alkyl, Pi–alkyl, *etc.*). The binding affinity and interaction characteristics of the selected compounds with the target enzymes are depicted in Table 5. The 2D and 3D docked poses, along with the interactions of the co-crystallized ligand, are illustrated in Fig. 9–14. The grid box with the *XYZ* dimensions 10.19 Å × 29.38 Å × −2.48 Å and

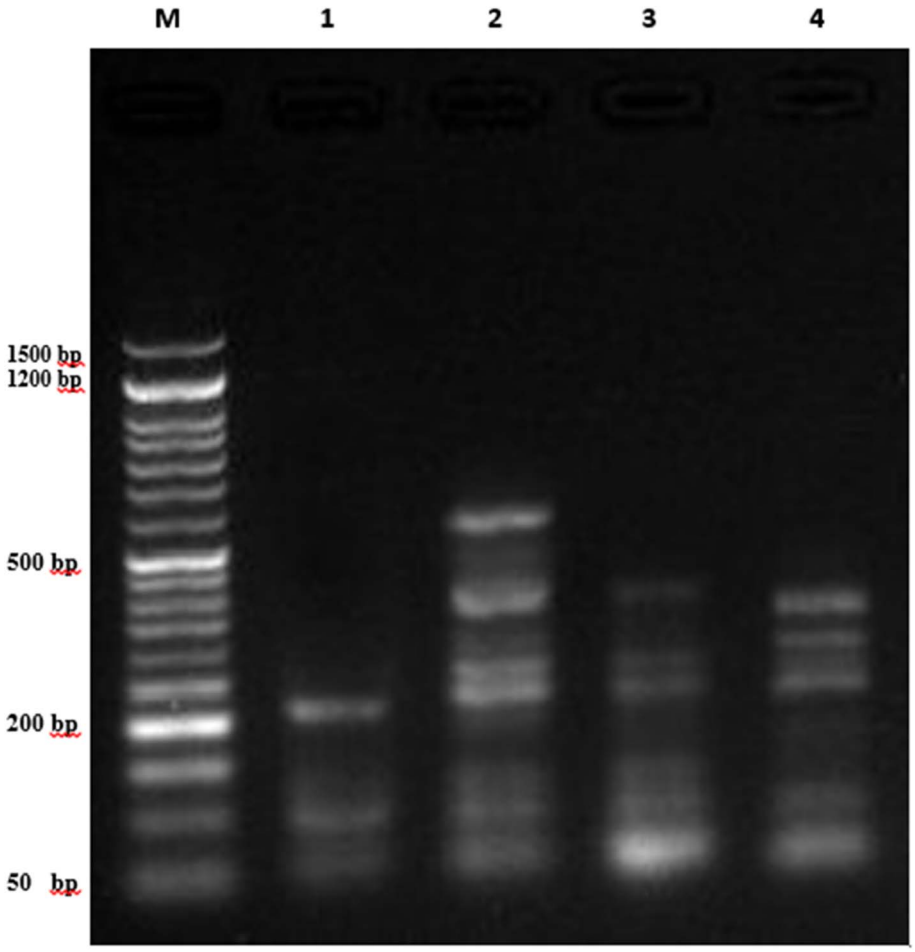

Fig. 7 DNA fragmentation detected with agarose gel in A549 cancer cell lines exposed to different compounds. M represents the DNA marker, Lane 1 represents the negative control of A549, Lane 2 represents A549 treated with **7a**, Lane 3 represents A549 treated with **7g**, and Lane 4 represents A549 treated with **Dox**.

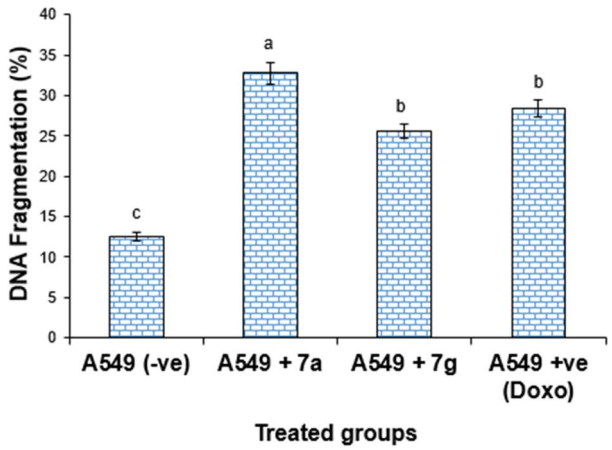

Fig. 8 DNA fragmentation detected in the lung cancer cell lines (A549) treated with different compounds **7a**, **7g** and **Dox**. Mean values with different superscripts ($^{a, b, c}$) between treatments in the same column are significantly different at $P < 0.05$.

Table 4 DNA fragmentation detected in the lung cancer cell lines in different treatment groups[a]

Treatment	DNA fragmentation% ($M \pm$ SEM)	Change	Inhibition%
A549 (−ve)	12.54 ± 0.45^{c}	0.00	0.00
A549 + **7a**	32.78 ± 1.35^{a}	20.24	27.78
A549 + **7g**	25.57 ± 0.94^{b}	13.03	17.74
A549 + **Dox**	28.38 ± 1.06^{b}	15.84	19.69

[a] Means with different superscripts ($^{a, b, c}$) between groups in the same column are significantly different at $P < 0.05$.

center 25.05, 19.72, 23.93 (*XYZ* coordinates) was defined to cover the 3-phosphoglycerate dehydrogenase binding while for the phosphoserine aminotransferase enzyme (PDB ID: 7T7J), the grid box was identified to cover pyridoxal-5′-phosphate (**PLP**) with dimensions 16.00 Å × 14.48 Å × 18.09 Å and a center 14.85, 5.89, 11.21 (*X*, *Y*, *Z*).

Assessment of the binding affinity of compounds 7a and 7g within the active site of human 3-phosphoglycerate dehydrogenase (PDB ID: 2G76)

Firstly, the docking setup was validated by the self-docking of the co-crystallized ligand **NAD** into the PHGDH active pocket

Table 5 Molecular docking results of the most active compounds **7a**, **7g**, and the co-crystalline ligand within the active pocket of 3-phosphoglycerate dehydrogenase (PHGDH) and phosphoserine aminotransferase (PSAT1)

Comp. no.	Score kcal mol^{-1}	Moieties from compounds	Amino acid residues	Type of interaction, distance Å
3-Phosphoglycerate dehydrogenase (PDB ID: 2G76)				
NAD	−7.7	CO	Thr77, Arg235	H-bonds 3.12, 2.99
		O–P═O	His205, Ser102, Arg154, Ile155, Gly156	H-bonds 3.12, 3.22, 3.25, 3.20, 2.86, 3.40
		NH_2, N	Ser211, Asp174	H-bonds 3.03, 3.37
		Phenyl ring	Arg235, Pro207	Alkyl
		CH_2	His205	Carbon–H bond
7a	−7.8	NO_2, N atoms of triazolo-triazine moiety	Ser211, His205, Asp174	H-bonds, 3.09, 2.84, 3.13
		Phenyl and triazine rings	Pro175, Pro207, Thr206	pi–alkyl, pi-sigma
		Triazole ring	Asp174	pi–anion
			Ile176, Gly153, Arg154	van der Walls
7g	−8.6	CO	Gly78	H-bond 2.33
		Phenyl and triazolo-triazine rings	Thr77, Ile155, Ala234, Pro207, Arg235	pi–donor H-bond, pi–alkyl
Phosphoserine aminotransferase (PDB ID: 7T7J)				
PLP	−6.5	CO, OH, O–P═O, N	Tr153, Lys198, Arg77, Gln197, Gly75, Asp174	H-bond 3.00, 2.72, 3.01, 2.98, 2.26, 2.85, 3.59
		P═O	Gly75	Carbon–hydrogen bond
			Trp102	van der Waals
7a	−7.4	NO_2	Ser177, Ser176, Thr153	H-bonds 3.23, 3.18, 2.93, 3.49
		NO, phenyl and triazolo-triazine rings	Trp102, Gln197, Arg77	Carbon hydrogen bond, pi–donor hydrogen bond, pi–pi stacked, pi–alkyl interactions
			Cys149	van der Waals
7g	−8.5	CO, N atom of triazine ring	Lys198, Trp102, Gly10	H-bond 3.19, 3.01, 3.09
		Phenyl and 4-chloro phenyl rings	Pro11, Phe80, Trp102, Arg77	pi–pi stacked, pi–alkyl
		Triazole ring	Lys198	pi–cation
			Gln197	van der Waals

(PDB ID: 2G76). The docking result indicates that the re-docked **NAD** was superimposed on the native ligand with a docking score of −7.7 kcal mol^{-1} and formed multiple interactions with the PHGDH active site (Fig. 9A and B). The **NAD** revealed intermolecular hydrogen bonds with Thr77, Arg235, His205, Ser102, Arg154, Ile155, Gly156, Ser211, and Asp174 and

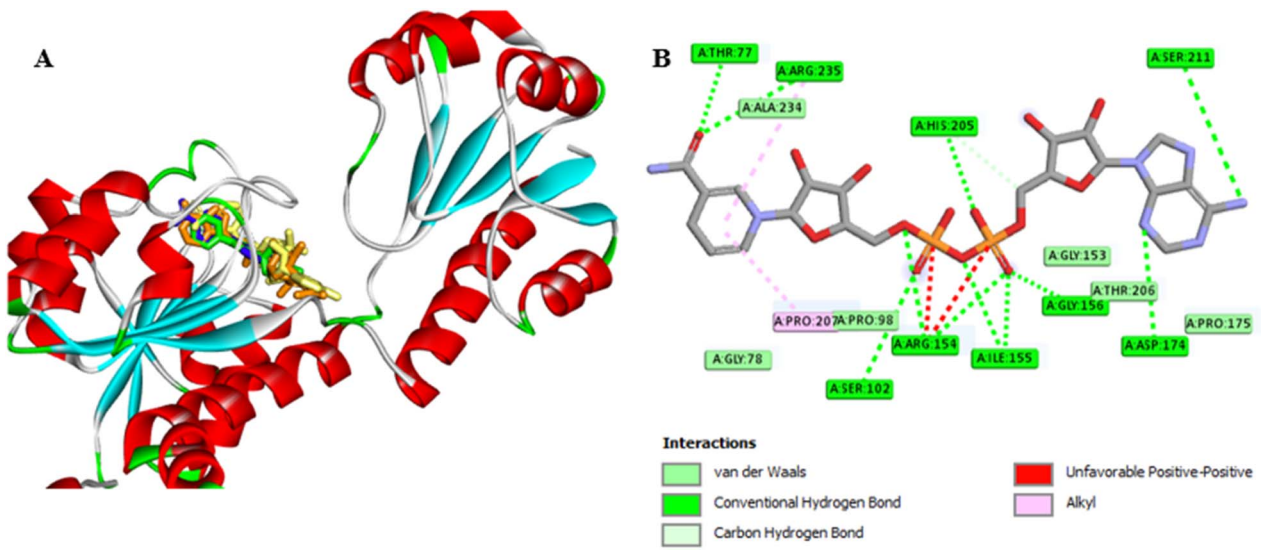

Fig. 9 (A) 3D conformations of the native (orange), re-docked ligand (yellow), compound **7a** (green), and compound **7g** (blue) within the active site of human 3-phosphoglycerate dehydrogenase (PDB ID: 2G76) indicating that they are superimposed in the same position. (B) 2D conformations of the re-docked co-crystalline ligand **NAD** within the active site of human 3-phosphoglycerate dehydrogenase (PDB ID: 2G76).

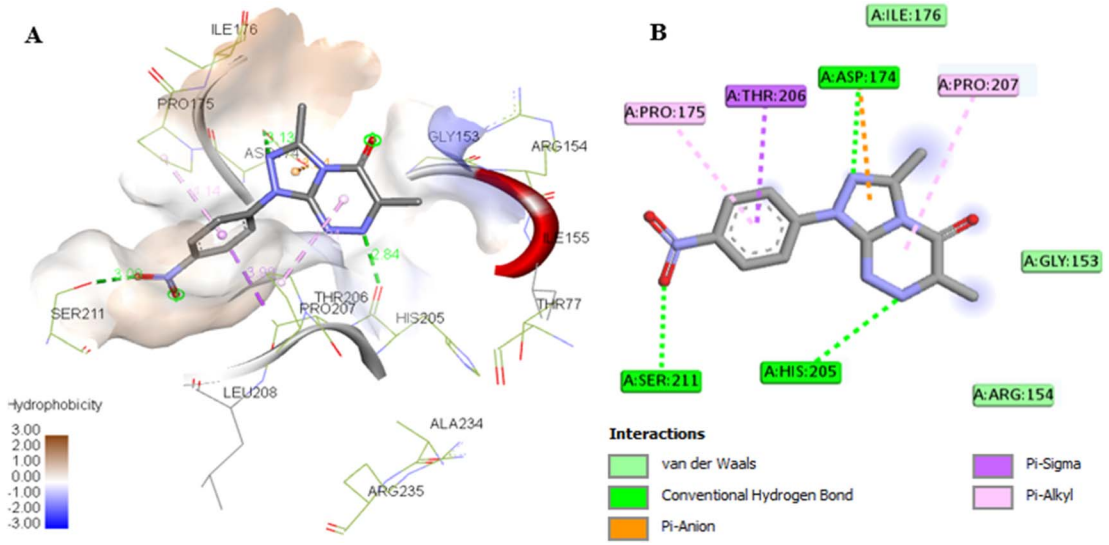

Fig. 10 (A) 3D conformations of compound **7a** within the active site of human 3-phosphoglycerate dehydrogenase (PDB ID: 2G76); (B) 2D conformations of compound **7a** within the active site of human 3-phosphoglycerate dehydrogenase (PDB ID: 2G76).

interacted *via* alkyl and carbon–hydrogen hydrophobic interactions with the Arg235, Pro207, and His205 amino acids of the binding site (Fig. 9B). Furthermore, compounds **7a** and **7g** were then docked into the PHGDH active site, which demonstrated better docking scores of −7.8 and −8.6 kcal mol^{-1} than **NAD**, respectively, and both of them were superimposed on the same position as the co-crystalline ligand (Table 5 and Fig. 9A). Compound **7a** formed a stable complex with the enzyme active pocket by establishing three hydrogen bonds with Ser211, His205, Asp174, Ile176, Gly153, and Arg154 residues, along with various hydrophobic π–alkyl, π–sigma, π–anion, and van der Waals interactions similar to the co-crystalline ligand (Fig. 10). On the other hand, compound **7g** exhibited one hydrogen bond with Gly78, in addition to the π-donor H-bond, π–alkyl with Thr77, Ile155, Ala234, Pro207, and Arg235 amino acids (Fig. 11).

Assessment of the binding affinity of compounds 7a and 7g within the active site of phosphoserine aminotransferase (PDB ID: 7T7J)

The co-crystallized ligand, pyridoxal-5′-phosphate (**PLP**), was re-docked into the active site of PSAT1, and the results showed that the re-docked **PLP** superimposed on the native ligand, achieving a docking score of −6.5 kcal mol^{-1} (Table 5 and Fig. 9A and B). Analysis of the binding site revealed that **PLP**

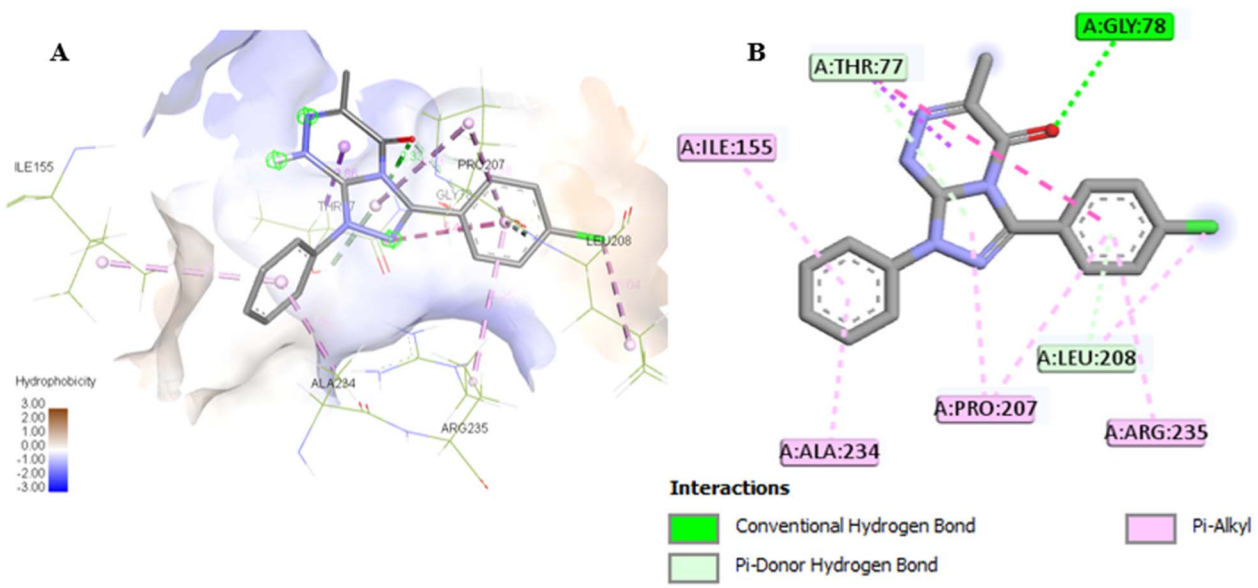

Fig. 11 (A) 3D conformations of compound **7g** within the active site of human 3-phosphoglycerate dehydrogenase (PDB ID: 2G76). (B) 2D conformations of compound **7g** within the active site of human 3-phosphoglycerate dehydrogenase (PDB ID: 2G76).

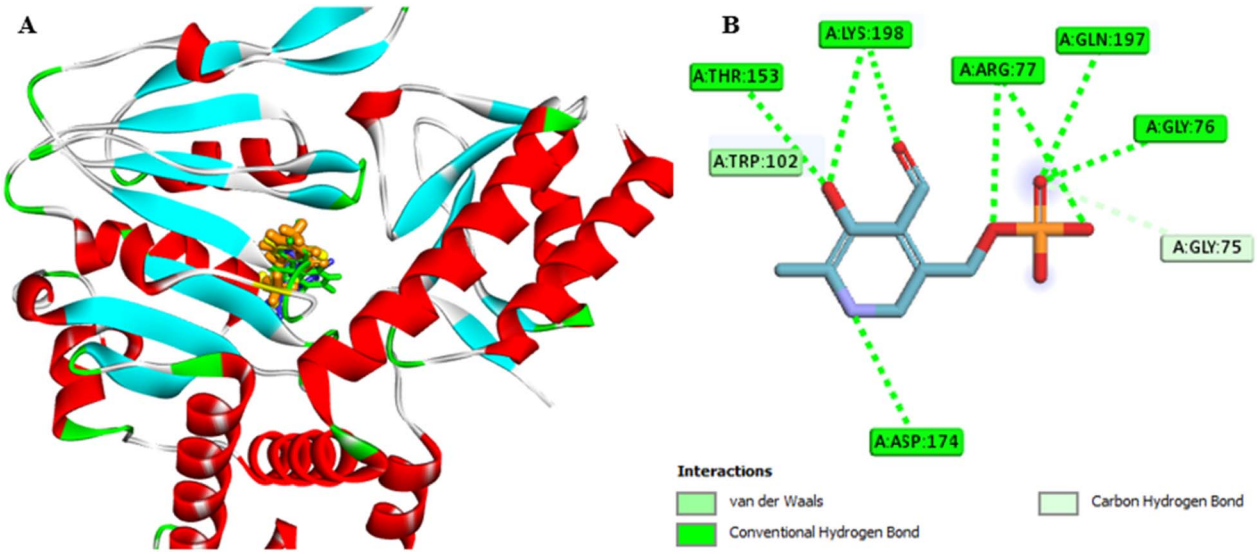

Fig. 12 (A) 3D conformations of the native (orange), re-docked ligand (yellow), compound **7a** (green), and compound **7g** (blue) within the active site of phosphoserine aminotransferase (PDB ID: 7T7J) indicating that they are superimposed in the same position. (B) 2D conformations of the re-docked co-crystalline ligand **PLP** within the active site of phosphoserine aminotransferase (PDB ID: 7T7J).

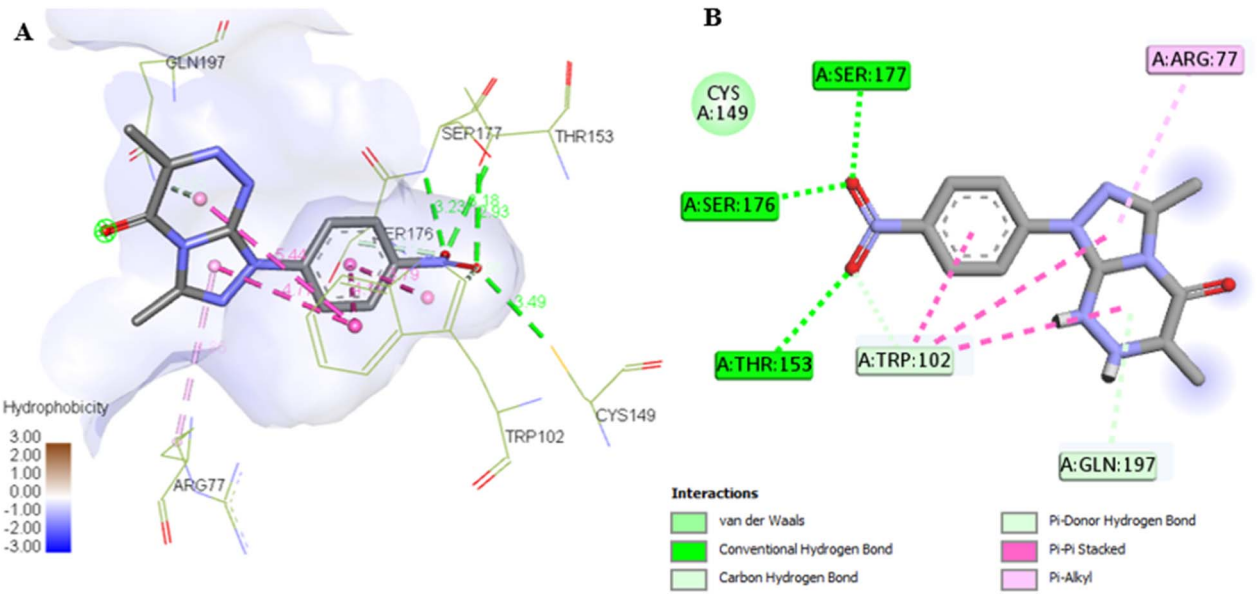

Fig. 13 (A) 3D conformations of compound **7a** within the active site of phosphoserine aminotransferase (PDB ID: 7T7J). (B) 2D conformations of compound **7a** within the active site of phosphoserine aminotransferase (PDB ID: 7T7J).

formed hydrogen bonds, a carbon H-bond, and van der Waals interactions with the amino acids Thr153, Lys198, Arg77, Gln197, Gly75, Asp174, and Trp102 (Table 5 and Fig. 12B).

The docking results for compounds **7a** and **7g** revealed docking scores of −7.4 and −8.5, respectively, outperforming the co-crystalline ligand **PLP**. Both compounds formed stable complexes with the PSAT1 active site and aligned with the same position as **PLP** (Table 5 and Fig. 12A). Compound **7a** established four hydrogen bonds with Ser177, Ser176, and Thr153, along with hydrophobic interactions involving Trp102, Gln197, Arg77, and Cys149 residues (Fig. 13). On the other hand, compound **7g** displayed three hydrogen bonds with Lys198, Trp102, and Gly10, in addition to the six pi–pi stacked, pi–alkyl, pi–cation, and van der Waals interactions with the amino acids Pro11, Phe80, Trp102, Arg77, Lys198, and Gln197 similar to the co-crystalline ligand (Fig. 14).

Materials and methods

Chemistry

Melting points were measured with an Electrothermal 9100 apparatus and were uncorrected. The IR spectra were recorded

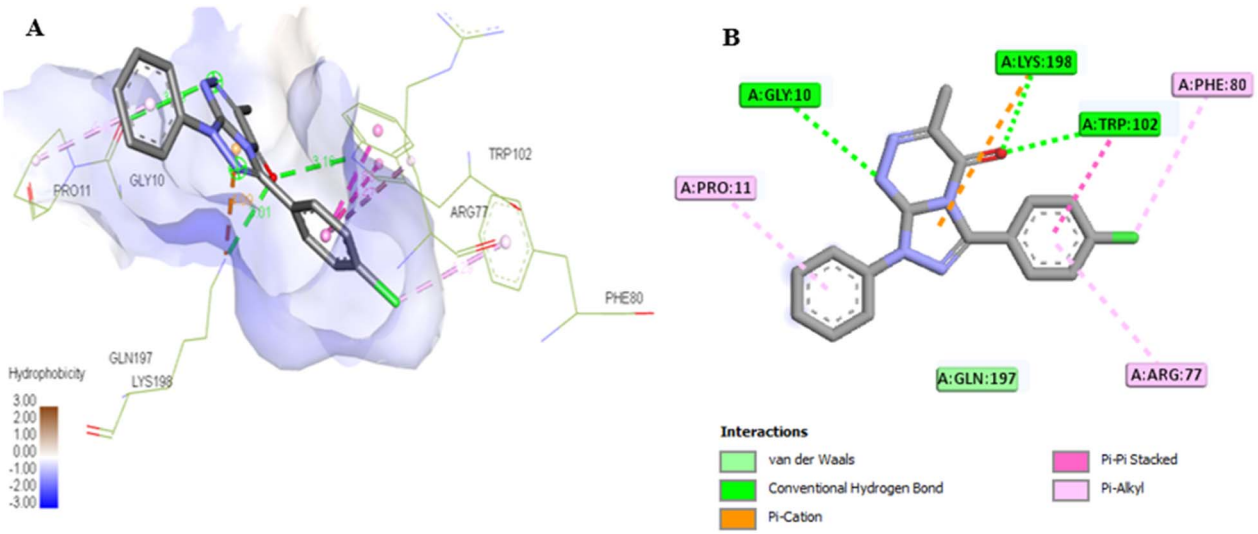

Fig. 14 (A) 3D conformations of compound **7g** within the active site of phosphoserine aminotransferase (PDB ID: 7T7J). (B) 2D conformations of compound **7g** within the active site of phosphoserine aminotransferase (PDB ID: 7T7J).

using a FTIR Bruker-vector 22 spectrophotometer and KBr pellets. The ^{1}H and ^{13}C NMR spectra were recorded in $CDCl_3$ or DMSO-d_6 as a solvent on the Varian Gemini NMR spectrometer at 300 MHz and 75 MHz, respectively. Chemical shifts were reported as δ values in ppm. The elemental analyses were performed at the Microanalytical Center, Cairo University. 6-Methyl-3-thioxo-3,4-dihydro-1,2,4-triazin-5(2*H*)-one **6** [16] and hydrazonoyl halides **1** [17–21] were prepared using the reported procedures.

Synthesis of 6-methyl-[1,2,4]triazolo[4,3-*b*][1,2,4]triazin-7(1*H*)-one derivatives (7a–j). To a mixture of hydrazonoyl halides **1a–j** (2 mmol) and 6-methyl-3-thioxo-3,4-dihydro-1,2,4-triazin-5(2*H*)-one **3** (0.29 g, 2 mmol) in chloroform (20 mL), triethylamine (0.2 mL, 2 mmol) was added. The reaction mixture was refluxed for 6 h and then cooled; the excess chloroform was removed under reduced pressure and the residue was treated with ethanol (10 mL). The precipitated solid was collected and crystallized from a suitable solvent to give [1,2,4]triazolo[4,3-*b*][1,2,4]triazin-7-one derivatives (**7a–j**). All the synthesized compounds and their physical properties are listed below:

*3,6-Dimethyl-1-(4-nitrophenyl)-[1,2,4]triazolo[4,3-b][1,2,4]triazin-7(1H)-one (**7a**).* Brown crystals (EtOH + DMF); mp 262–264 °C; yield (67%); ^{1}H NMR (300 MHz, DMSO-d_6) δ 2.32 (s, 3H, CH_3), 2.58 (s, 3H, CH_3), 8.38 (d, 2H, 4-$NO_2C_6H_4$, $J \approx 9$ Hz), 8.47 (d, 2H, 4-$NO_2C_6H_4$, $J \approx 9$ Hz); ^{13}C NMR (75 MHz, DMSO-d_6) δ 16.5, 18.4, 118.9, 124.5, 138.9, 145.7, 151.8, 153.0, 155.3, 161.7. Anal. calcd for $C_{12}H_{10}N_6O_3$ (286.25), C, 50.35; H, 3.52; N, 29.36. Found, C, 50.46; H, 3.39; N, 29.47.

*3-Ethyl-6-methyl-1-(4-nitrophenyl)-[1,2,4]triazolo[4,3-b][1,2,4]triazin-7(1H)-one (**7b**).* Brown crystals (EtOH); mp 200–202 °C; yield (69%). ^{1}H NMR (300 MHz, $CDCl_3$) δ 1.48 (t, 3H, $CH_2C\underline{H}_3$, $J \approx 8$ Hz), 2.45 (s, 3H, CH_3), 3.03 (q, 2H, $C\underline{H}_2CH_3$, $J \approx 8$ Hz), 8.30 (d, 2H, 4-$NO_2C_6H_4$, $J \approx 9$ Hz), 8.45 (d, 2H, 4-$NO_2C_6H_4$, $J \approx 9$ Hz); ^{13}C NMR (75 MHz, $CDCl_3$) δ 9.7, 17.5, 18.2, 119.5, 124.7, 141.0, 145.2, 147.9, 148.0, 155.7, 161.5. Anal. calcd for $C_{13}H_{12}N_6O_3$ (300.28), C, 52.00; H, 4.03; N, 27.99. Found, C, 52.11; H, 4.15; N, 27.86.

*6-Methyl-1-(4-nitrophenyl)-3-propyl-[1,2,4]triazolo[4,3-b][1,2,4]triazin-7(1H)-one (**7c**).* Brown crystals (DMF); mp 202–204 °C; yield (64%). ^{1}H NMR (300 MHz, $CDCl_3$) δ 1.13 (t, 3H, CH_2CH_2-$C\underline{H}_3$, $J \approx 8$ Hz), 1.91–1.99 (m, 2H, $CH_2C\underline{H}_2CH_3$), 2.48 (s, 3H, CH_3), 3.00 (t, 2H, $C\underline{H}_2CH_2CH_3$, $J \approx 8$ Hz), 8.34 (d, 2H, 4-$NO_2C_6H_4$, $J \approx 9$ Hz), 8.49 (d, 2H, 4-$NO_2C_6H_4$, $J \approx 9$ Hz); ^{13}C NMR (75 MHz, $CDCl_3$) δ 13.6, 18.4, 19.2, 25.6, 119.7, 124.9, 141.2, 145.5, 147.0, 148.1, 156.0, 161.6. Anal. calcd for $C_{14}H_{14}N_6O_3$ (314.31), C, 53.50; H, 4.49; N, 26.74. Found, C, 53.61; H, 4.37; N, 26.87.

*3-Isopropyl-6-methyl-1-(4-nitrophenyl)-[1,2,4]triazolo[4,3-b][1,2,4]triazin-7(1H)-one (**7d**).* Brown crystals (EtOH); mp 208–210 °C; yield (66%). ^{1}H NMR (300 MHz, $CDCl_3$) δ 1.52 (d, 6H, $CH(C\underline{H}_3)_2$, $J \approx 7$ Hz), 2.47 (s, 3H, CH_3), 3.43–3.52 (m, 1H, $CH(CH_3)_2$), 8.32 (d, 2H, 4-$NO_2C_6H_4$, $J \approx 9$ Hz), 8.48 (d, 2H, 4-$NO_2C_6H_4$, $J \approx 9$ Hz); ^{13}C NMR (75 MHz, $CDCl_3$) δ 18.3, 19.1, 24.9, 119.6, 124.7, 141.1, 145.2, 148.1, 150.9, 155.6, 161.5. Anal. calcd for $C_{14}H_{14}N_6O_3$ (314.31), C, 53.50; H, 4.49; N, 26.74. Found, C, 53.60; H, 4.38; N, 26.86.

*3-Isobutyl-6-methyl-1-(4-nitrophenyl)-[1,2,4]triazolo[4,3-b][1,2,4]triazin-7(1H)-one (**7e**).* Brown crystals (EtOH); mp 202–204 °C; yield (63%). ^{1}H NMR (300 MHz, $CDCl_3$) δ 1.12 (d, 6H, $CH_2CH(C\underline{H}_3)_2$, $J \approx 7$ Hz), 2.30–2.39 (m, 1H, $CH_2C\underline{H}(CH_3)_2$), 2.48 (s, 3H, CH_3), 2.93 (d, 2H, $C\underline{H}_2CH(CH_3)_2$, $J \approx 7$ Hz), 8.36 (d, 2H, 4-$NO_2C_6H_4$, $J \approx 9$ Hz), 8.50 (d, 2H, 4-$NO_2C_6H_4$, $J \approx 9$ Hz); ^{13}C NMR (75 MHz, $CDCl_3$) δ 18.4, 22.3, 26.4, 32.2, 94.7, 119.7, 124.9, 141.1, 145.5, 146.4, 156.0, 161.6. Anal. calcd for $C_{15}H_{16}N_6O_3$ (328.33), C, 54.87; H, 4.91; N, 25.60. Found, C, 54.99; H, 4.79; N, 25.72.

*6-Methyl-1-phenyl-3-(p-tolyl)-[1,2,4]triazolo[4,3-b][1,2,4]triazin-7(1H)-one (**7f**).* Beige crystals (DMF); mp 250–252 °C; yield (72%). ^{1}H NMR (300 MHz, $CDCl_3$) δ 2.47 (s, 3H, CH_3), 2.53 (s, 3H, CH_3), 7.33–7.38 (m, 3H, Ar-H), 7.51 (t, 2H, Ar-H, $J \approx 8$ Hz), 8.18–8.24

(m, 4H, Ar-H); ^{13}C NMR (75 MHz, $CDCl_3$) δ 18.4, 20.9, 121.6, 125.1, 126.4, 128.7, 129.2, 131.5, 138.5, 140.9, 147.9, 151.4, 152.8, 161.7. Anal. calcd for $C_{18}H_{15}N_5O$ (317.35), C, 68.13; H, 4.76; N, 22.07. Found, C, 68.25; H, 4.63; N, 22.18.

*3-(4-Methoxyphenyl)-6-methyl-1-phenyl-[1,2,4]triazolo[4,3-b][1,2,4]triazin-7(1H)-one (**7g**).* White crystals (DMF); mp 256–258 °C; yield (70%). ^{1}H NMR (300 MHz, DMSO-d_6) δ 2.34 (s, 3H, CH_3), 3.87 (s, 3H, OCH_3), 7.20 (d, 2H, Ar-H, $J \approx 9$ Hz), 7.42 (t, 1H, Ar-H, $J \approx 8$ Hz), 7.60 (t, 2H, Ar-H, $J \approx 8$ Hz), 8.12 (d, 2H, Ar-H, $J \approx 9$ Hz), 8.19 (d, 2H, Ar-H, $J \approx 9$ Hz); ^{13}C NMR (75 MHz, DMSO-d_6) δ 18.2, 55.5, 113.8, 120.7, 122.8, 126.3, 128.9, 130.8, 138.4, 147.9, 151.4, 152.6, 160.4, 161.8. Anal. calcd for $C_{18}H_{15}N_5O_2$ (333.35), C, 64.86; H, 4.54; N, 21.01. Found, C, 64.98; H, 4.41; N, 21.14.

*3-(4-Chlorophenyl)-6-methyl-1-phenyl-[1,2,4]triazolo[4,3-b][1,2,4]triazin-7(1H)-one (**7h**).* Yellow crystals (DMF); mp 245–247 °C; yield (74%). ^{1}H NMR (300 MHz, $CDCl_3$) δ 2.54 (s, 3H, CH_3), 7.38 (t, 1H, Ar-H, $J \approx 8$ Hz), 7.49–7.58 (m, 4H, Ar-H), 8.22 (d, 2H, Ar-H, $J \approx 8$ Hz), 8.31 (d, 2H, Ar-H, $J \approx 9$ Hz); ^{13}C NMR (75 MHz, $CDCl_3$) δ 18.6, 120.4, 122.0, 127.5, 128.0, 129.3, 131.9, 136.0, 138.1, 148.0, 151.9, 155.9, 161.9. Anal. calcd for $C_{17}H_{12}ClN_5O$ (337.77), C, 60.45; H, 3.58; N, 20.73. Found, C, 60.57; H, 3.72; N, 20.86.

*3-(Furan-2-yl)-6-methyl-1-(4-nitrophenyl)-[1,2,4]triazolo[4,3-b][1,2,4]triazin-7(1H)-one (**7i**).* Pale brown crystals (CH_3CN); mp 269–271 °C; yield (71%). ^{1}H NMR (300 MHz, DMSO-d_6) δ 2.39 (s, 3H, CH_3), 6.87–6.89 (m, 1H, furyl-H), 7.66 (d, 1H, furyl-H, $J \approx 3$ Hz), 8.15 (d, 1H, furyl-H, $J \approx 1$ Hz), 8.41–8.49 (m, 4H, 4-$NO_2C_6H_4$); ^{13}C NMR (75 MHz, DMSO-d_6) δ 18.2, 112.6, 117.1, 119.8, 125.3, 136.5, 137.4, 141.2, 145.0, 147.1, 148.3, 154.9, 160.8. Anal. calcd for $C_{15}H_{10}N_6O_4$ (338.28), C, 53.26; H, 2.98; N, 24.84. Found, C, 53.38; H, 2.86; N, 24.95.

*6-Methyl-1-(4-nitrophenyl)-3-(thiophen-2-yl)-[1,2,4]triazolo[4,3-b][1,2,4]triazin-7(1H)-one (**7j**).* Pale brown crystals (DMF); mp 242–244 °C; yield (69%). ^{1}H NMR (300 MHz, DMSO-d_6) δ 2.38 (s, 3H, CH_3), 7.36 (t, 1H, thieny-H, $J \approx 5$ Hz), 8.05 (d, 1H, thieny-H, $J \approx 5$ Hz), 8.22 (d, 1H, thieny-H, $J \approx 5$ Hz), 8.38–8.47 (m, 4H, 4-$NO_2C_6H_4$); ^{13}C NMR (75 MHz, DMSO-d_6) δ 18.3, 119.7, 120.4, 123.4, 125.3, 128.6, 131.7, 132.2, 139.9, 141.1, 144.9, 154.8, 160.8. Anal. calcd for $C_{15}H_{10}N_6O_3S$ (354.34), C, 50.84; H, 2.84; N, 23.72. Found, C, 50.95; H, 2.71; N, 23.85.

Anti-cancer activity

MTT cytotoxicity assay. Cell viability was tested using the MTT assay, 3-(4,5-dimethylthiazol-2-yl)-2,5-diphenyl-tetrazolium bromide (Bio Basic Canada Inc. Toronto, Canada).[26] Under class II biosafety regulations, the procedures were carried out in a sterile laminar air flow cabinet (Baker, SG403INT; Sanford, ME, USA). Cell lines were obtained from the American type culture collection (ATCC) as a gift from Dr Stig Linder, Karonisca Institute, Sweden. All incubations were performed at 37 °C in a 5% CO_2 incubator with a 95% humidified environment (Sheldon, TC2323; Cornelius, OR, USA). 96-well micro titer polypropylene plates were seeded with cells at a density of 10^4 cells per well in complete DMEM media, and the cells were allowed to adhere for 24 hours. After the media was aspirated, the tested compounds were added to the cells in a single dose of 100 μg ml^{-1} in DMSO. Each well received 40 μl of MTT salt (2.5 g ml^{-1}) following a 48 hour incubation period. 200 μl of 10% sodium dodecyl sulfate (SDS) was added to each well after the reaction ended, and any formazan crystals that could have been produced were dissolved by two hours of incubator heating to 37 °C. The amount of formazan product was measured at 595 nm using a microplate reader (Bio-Rad Laboratories, model 3350, California, USA) with a reference wavelength of 690 nm, serving as a backdrop. Rather than the drugs under investigation, the medium was applied to the untreated cells (negative control). The examined compounds were dissolved in dimethylsulfoxide (DMSO), and the final concentration in the cells was less than 0.2%. For each compound and the control, the solvent concentration was the same. By applying different concentrations of 0, 6.25, 12.2, 25, and 50 μg ml^{-1} (three replicates), the concentration required for 50% inhibition of cell viability (IC_{50}) was estimated for the potential compounds, which demonstrated preliminary cytotoxic effects at 100 μg ml^{-1}.

Gene expression analysis

Quantitative real-time PCR method

RNA isolation and reverse transcription (RT) reaction. The RNeasy Mini Kit (Qiagen, Hilden, Germany), augmented with a DNaseI (Qiagen) digestion step, was employed to extract total RNA from lung cancer cell lines following the manufacturer's procedure. The isolated total RNA was treated with one unit of RQ1 RNAse-free DNAse (Invitrogen, Germany) to eliminate DNA remnants, re-suspended in DEPC-treated water, and quantified photometrically at 260 nm. The purity of total RNA was evaluated using the 260/280 nm ratio, which ranged from 1.8 to 2.1.[27]

Furthermore, integrity was confirmed using ethidium bromide-stained examination of 28S and 18S bands *via* formaldehyde-containing agarose gel electrophoresis. Aliquots were utilized immediately for reverse transcription (RT); otherwise, they were preserved at −80 °C.

The poly(A) + RNA extracted from the lung cancer cell lines was reverse transcribed into the cDNA in a total amount of 20 μl utilizing the Revert Aid TM First Strand cDNA Synthesis Kit (Fermentas, Germany). A total of 5 μg of RNA was utilized with a master mix. The master mix comprised 50 mM $MgCl_2$, 10× RT buffer (50 mM KCl; 10 mM Tris–HCl; pH 8.3), 10 mM of each dNTP, 50 μM oligo-dT primer, 20 IU ribonuclease inhibitor (50 kDa recombinant enzyme to suppress RNase activity), and 50 IU MuLV reverse transcriptase. Each sample mixture was centrifuged for 30 seconds at 1000 g and thereafter transferred to the thermocycler. The RT reaction was conducted at 25 °C for 10 minutes, subsequently at 42 °C for 1 hour, and concluded with a denaturation phase at 99 °C for 5 minutes. Subsequently, the reaction tubes containing RT-prepared samples were rapidly chilled in an ice chamber prior to cDNA amplification *via* the quantitative real-time polymerase chain reaction (qRT-PCR).

Quantitative real-time-PCR (qRT-PCR). The cDNA copy number of lung cancer cell lines was determined using the StepOne™ Real-Time PCR System from Applied Biosystems (Thermo Fisher Scientific, Waltham, MA, USA).

Table 6 Primer sequences used for the qRT-PCR of lung cancer cell lines[a]

Gene	Primer sequence	GenBank (accession no.)
BCL-2	F: TTCCGCGTGATTGAAGACAC R: ACTTCATCACTATCTCCCGGT	KY098818.1
p53	F: GGAAATCTCACCCCATCCCA R: CAGTAAGCCAAGATCACGCC	AB082923.1
BAX	F: AACATGGAGCTGCAGAGGAT R: CCAATGTCCAGCCCATGATG	L22474.1
GAPDH	F: AGGTCGGAGTCAACGGATTT R:ATCGCCCCACTTGATTTTGG	NM_001357943.2

[a] BCL-2: B-cell lymphoma-2 gene; BAX: BCL-2-associated X protein-encoding gene; p53: tumor suppressor gene; GAPDH: glyceraldehyde-3-phosphate dehydrogenase.

The PCR reactions were prepared in 25 μl mixes comprising 12.5 μl of 1× SYBR® Premix Ex Taq™ (TaKaRa, Biotech. Co. Ltd), 0.5 μl of 0.2 μM sense primer, 0.5 μl of 0.2 μM antisense primer, 6.5 μl of distilled water, and 5 μl of cDNA template.

The reaction protocol was divided into three stages. The initial step was conducted at 95 °C for a duration of 3 minutes. The second step comprised 40 cycles, each divided into three phases: (a) 95 °C for 15 seconds, (b) 55 °C for 30 seconds, and (c) 72 °C for 30 seconds. The third stage comprised 71 cycles, first at 60 °C and subsequently increasing by approximately 0.5 °C every 10 seconds until 95 °C. Every experiment incorporated a distilled water control. The particular primer sequences for the lung cancer cell lines (BCL-2, BAX, and p53 genes, Brito *et al.*, 2012)[28] were created and are presented in Table 6. A melting curve analysis was conducted at 95.0 °C after each qPCR to assess the quality of the utilized primers. The relative quantification of the target gene to the reference gene was assessed using the $2^{-\Delta\Delta C_T}$ method.[29–31]

DNA damage evaluation using the comet assay

The determination of DNA damage *via* the comet assay was conducted using lung cancer cell lines, following the methodology established by Olive *et al.* (1990).[32] Following trypsin treatment to generate a single-cell suspension, approximately 1.5×10^4 cells were embedded in 0.75% low-gelling-temperature agarose and swiftly pipetted onto a pre-coated microscope slide.

The samples underwent lysis for 4 hours at 50 °C in a solution containing 0.5% SDS and 30 mM EDTA at pH 8.0. Following an overnight rinse at room temperature in a Tris/borate/EDTA buffer, pH 8.0, samples underwent electrophoresis for 25 minutes at 0.6 V cm^{-1} and were subsequently stained with propidium iodide. The slides were examined with a fluorescence microscope equipped with a CCD camera, and 150 individual comet images were analyzed from each sample for a tail moment, DNA content, and percentage of DNA in the tail. Approximately 100 cells were analyzed per sample to assess the percentage of cells exhibiting comet-like DNA damage.

The non-overlapping cells were randomly selected and assigned a score on a scale of 0–3 based on the comet tail length migration and the relative proportion of DNA in the nucleus. Class 0 indicates no detectable DNA damage and no tail; class 1 indicates a tail length less than the diameter of the nucleus; class 2 indicates a tail length between 1× and 2× the nuclear diameter; and class 3 indicates a tail longer than 2× the diameter of the nucleus (Collins *et al.*, 1997).[33]

DNA fragmentation assay

DNA gel electrophoresis laddering assay. The DNA fragmentation assay in lung cancer cell lines was performed in accordance with the protocol established by Yawata (1998)[34] with some modifications. Briefly, the lung cancer cell lines (A549) exposed to different compounds such as PT1, PT7 and Doxorubicin were homogenized in 1 ml of the medium and centrifuged (10 min at 800 rpm). The low-molecular-weight genomic DNA was extracted as described in Yawata (1998).[34] Approximately 1×10^6 cells of each treatment were plated. All the cells (including floating cells) were harvested and washed with Dulbecco's phosphate buffered saline. The cancer cells were lysed with the lysis buffer containing 10 mM Tris (pH 7.4), 150 mM NaCl, 5 mM ethylenediaminetetraacetic acid (EDTA), and 0.5% Triton X-100 for 30 min on ice. Lysates were vortexed and cleared by centrifugation at 10 000 g for 20 min. Fragmented DNA in the supernatant was extracted with an equal volume of a neutral phenol : chloroform : isoamyl alcohol mixture (25 : 24 : 1) and analyzed electrophoretically on 2% agarose gels containing 0.1 μg ml^{-1} ethidium bromide.

Diphenylamine reaction procedure

The lung cancer cell lines (A549) were used to determine the quantitative profile of the DNA fragmentation. The cell lines were collected immediately after the culture and treatment with PT1 and PT7 as well as with **Dox**. The cancer cells were lysed in 0.5 ml of lysis buffer containing 10 mM Tris–HCl (pH 8), 1 mM EDTA, and 0.2% Triton X-100 and centrifuged at 10 000 rpm (Eppendorf) for 20 min at 4 °C. The pellets were re-suspended in 0.5 ml of lysis buffer. To the pellets (P) and the supernatants (S), 0.5 ml of 25% tri-chloroacetic acid (TCA) was added and incubated at 4 °C for 24 h. The cells were then centrifuged for 20 min at 10 000 rpm (Eppendorf) at 4 °C and the pellets were suspended in 80 ml of 5% TCA, followed by incubation at 83 °C for 20 min. Subsequently, to each cell sample, 160 ml of diphenylamine (DPA) solution [150 mg DPA in 10 ml glacial acetic acid, 150 ml of sulfuric acid and 50 ml acetaldehyde (16 mg ml^{-1})] was added and incubated at room temperature for 24 h (Gibb *et al.*,[35] 1997). The proportion of the fragmented DNA was calculated from the absorbance values at 600 nm wavelength using the formula:

$$\%\ \text{fragmented DNA} = [\text{OD(S)}/[\text{OD(S)} + \text{OD(P)}]] \times 100$$

(OD: optical density, S: supernatants, P: pellets).

Statistical analysis

All data were analyzed using the General Linear Model (GLM) procedure of the Statistical Analysis System (SAS) (1982),[36] followed by the Scheffé-test to assess significant differences

between groups. The values are expressed as mean ± SEM. All statements of significance were based on a probability of $P < 0.05$.

Molecular docking simulation

The molecular docking of the most active compounds **7a** and **7g** with two enzymes that play an important role in lung cancer progression, namely, 3-phosphoglycerate dehydrogenase (PHGDH) and phosphoserine aminotransferase (PSAT1), was performed on Autodock 4 in PyRx software version 8.[37,38] The 3D structures of the target enzymes were obtained from the RCSB protein data bank in the PDB format using codes 2G76 (3-phosphoglycerate dehydrogenase in complex with nicotinamide–adenine–dinucleotide (**NAD**)) and 7T7J (phosphoserine aminotransferase in complex with pyridoxal-5′-phosphate (**PLP**)).[39,40]

Before the docking process, the enzymes underwent preparation, including removal of the co-crystallized ligands and water molecules, then optimization using the *QuickPrep* tool module in the MOE program. The resulting files were saved as pdb and then converted to the PDBQT format using Autodock Vina tools. Autodock tools were employed to set the size and the center of the grid box that covers the native ligands completely. The docking protocol was validated by re-docking the co-crystallized ligands into the enzyme-active sites and the RMSD was calculated using the DockRMSD server.[41] The chemical structure of the selected compounds **7a** and **7g** were constructed with the *ChemDraw* ultra-10.0, saved as SDF files, then minimized by applying the MMFF94 force field and converted to pdbqt files using OpenBable tools involved in PyRx software. PyRx software presented the 8 most suitable docking poses of the ligand–protein complex after the docking was completed and subsequently ranked according to the binding energy. We selected the first docking pose, which is the most suitable pose where the ligands have the lowest binding energy, zero Å root-mean-square deviation (RMSD) and strongly interact with the protein's catalytic cavity, and visualized using BIOVIA Discovery Studio Visualizer 2021 for insights into the ligand binding position in the protein cavity.

Crystallography

The data for compound **7b** was collected at a low temperature (100 K) on a Rigaku XtaLAB Synergy dual microfocus X-ray diffractometer, using a PhotonJet-S series of microfocus X-ray source, Cu-Kα radiation ($\lambda = 1.54184$ Å) and equipped with an Oxford Cryosystems Cooler Device. The cell parameters of the final unit were obtained by means of a least-squares refinement. The structure was solved by Direct Methods using SHELXT 2018/2 (ref. 42) and refined by means of least-squares procedures on a F^2 using the program CRYSTALS.[43] The Atomic Scattering Factors were taken from the International Tables for X-Ray Crystallography.[44] All hydrogen atoms were geometrically placed and refined using a riding model.

All non-hydrogen atoms were anisotropically refined, and in the last cycles of refinement, a weighting scheme was used, where weights are calculated from the following formula:

$$w = 1/[2(\mathrm{Fo2}) + (\mathrm{aP})2 + \mathrm{bP}]$$

where $P = (\mathrm{Fo2} + 2\mathrm{Fc2})/3$. Molecules were drawn with the program ORTEP32 with 30% probability displacement ellipsoids for non-hydrogen atoms.[45]

Conclusions

In summary, we reported a novel series of [1,2,4]triazolo[4,3-*b*][1,2,4]triazin-7-one derivatives (**7a–j**) by the reaction of 6-methyl-3-thioxo-3,4-dihydro-1,2,4-triazin-5(2*H*)-one with the corresponding hydrazonoyl halides in chloroform. The chemical structures of these compounds were proven using spectral data, elemental analyses, and single-crystal X-ray diffraction. The anti-cancer activity of these compounds was determined against the PC3, A549, PACA2 and BJ1 using MTT assay. Two compounds, **7a** and **7g**, showed potent anti-cancer activities with low IC_{50} values (36.6 and 40.1 μM, respectively) compared to the reference drug with an IC_{50} value of 43.8 μM on lung cell lines and demonstrated safe mortality effect on the normal cell line (BJ1) with cytotoxicity percentages of 3.5% and 2.8%, respectively. These compounds (**7a** and **7g**) were investigated further to determine their mechanism of action using DNA fragmentation, DNA damage and gene expression (BCL-2, BAX, and p53 genes). Molecular docking was employed to explore the binding affinity between the most active compounds (**7a** and **7g**) and two key enzymes, PHGDH and PSAT1, which play vital roles in the progression of lung cancer.

Data availability

The data supporting this article (copies of ^{1}H, ^{13}C NMR spectra and single-crystal X-ray details) have been included as part of the ESI.†

Conflicts of interest

There are no conflicts to declare.

References

1 R. Aggarwal and G. Sumran, An insight on medicinal attributes of 1,2,4-triazoles, *Eur. J. Med. Chem.*, 2020, **205**, 112652.
2 P. Yang, X. Zheng, G. Zhang, C. Lei, G. Cheng and H. Yang, Construction of heterocycle-triazolotriazine framework energetic compounds: towards novel high-performance explosives, *Chem. Commun.*, 2024, **60**, 10588–10591.
3 Q. Wang, Y. Shao and M. Lu, Amino-tetrazole functionalized fused triazolo-triazine and tetrazolo-triazine energetic materials, *Chem. Commun.*, 2019, **55**, 6062–6065.
4 G. Zhang, W. Hu, J. Ma, H. Yang and G. Cheng, Combining 5,6-fused triazolo-triazine with pyrazole: A novel energetic framework for heat-resistant explosive, *Chem. Eng. J.*, 2021, **426**, 131297.
5 M. Mojzych, P. Tarasiuk, Z. Karczmarzyk, M. Juszczak, W. Rzeski, A. Fruzinski and A. Wozny, Synthesis, Structure and Antiproliferative Activity of New pyrazolo[4,3- e]triazolo

[4,5-b][1,2,4]triazine Derivatives, *Med. Chem.*, 2018, **14**, 53–59.

6 H. Peng, G. Kumaravel, G. Yao, L. Sha, J. Wang, H. Van Vlijmen, T. Bohnert, C. Huang, C. B. Vu, C. L. Ensinger, H. Chang, T. M. Engber, E. T. Whalley and R. C. Petter, Novel Bicyclic Piperazine Derivatives of Triazolotriazine and Triazolopyrimidines as Highly Potent and Selective Adenosine A2A Receptor Antagonists, *J. Med. Chem.*, 2004, **47**, 6218–6229.

7 Y. Guo, X. Peng, Y. Ji, Y. Zhang, J. Ding, Z. Zhan, J. Ai and W. Duan, Synthesis of triazolotriazine derivatives as c-Met inhibitors, *Mol. Diversity*, 2020, **25**, 839–846.

8 F. Akahoshi, S. Takeda, T. Okada, M. Kajii, H. Nishimura, M. Sugiura, Y. Inoue, C. Fukaya, Y. Naito, T. Imagawa and N. Nakamura, Synthesis and Pharmacological Activity of Triazolo[1,5-a]triazine Derivatives Inhibiting Eosinophilia, *J. Med. Chem.*, 1998, **41**, 2985–2993.

9 A. A. Thai, B. J. Solomon, L. V. Sequist, J. F. Gainor and R. S. Heist, Lung cancer, *Lancet*, 2021, **398**, 535–554.

10 B. Cheng, S. Xiong, C. Li, H. Liang, Y. Zhao, J. Li, J. Shi, L. Ou, Z. Chen, P. Liang, W. Liang and J. He, An annual review of the remarkable advances in lung cancer clinical research in 2019, *J. Thorac. Dis.*, 2020, **12**, 1056–1069.

11 N. Samanci and E. Celik, The top 100 cited articles in lung cancer – a bibliometric analysis, *Wspólcz. Onkol.*, 2020, **24**, 17–28.

12 M. F. Mridha, A. R. Prodeep, A. S. M. M. Hoque, M. R. Islam, A. A. Lima, M. M. Kabir, M. A. Hamid, Y. Watanobe and R. Morales, A Comprehensive Survey on the Progress, Process, and Challenges of Lung Cancer Detection and Classification, *J. Healthc. Eng.*, 2022, **2022**, 1–43.

13 T. Barr, S. Ma, Z. Li and J. Yu, Recent advances and remaining challenges in lung cancer therapy, *Chin. Med. J.*, 2024, **137**, 533–546.

14 G. S. Jones and D. R. Baldwin, Recent advances in the management of lung cancer, *Clin. Med.*, 2018, **18**, s41–s46.

15 L. Scharnetzki and J. H. Schiller, Lung Cancer, *Chest*, 2021, **159**, 1721–1722.

16 E. A. Falco, E. Pappas and G. H. Hitchings, 1,2,4-Triazine Analogs of the Natural Pyrimidines, *J. Am. Chem. Soc.*, 2002, **78**, 1938–1941.

17 H. M. Hassaneen, H. A. H. Mousa, N. M. Abed and A. S. Shawali, Chemistry of C-Heteroarylhydrazidoyl Halides. Synthesis and Reactions of N-(p-Nitrophenyl)-C-(2-thienyl)-formohydrazidoyl Halides, *Heterocycles*, 1988, **27**, 695.

18 T. Katada, S. Eguchi and T. Sasaki, Thermal cycloaddition reactions of thiocarbonyl compounds. Part 2. 1,3-dipolar cycloaddition reactions of adamantanethione with nitrile oxides, nitrilimines, and diazoalkanes, *J. Chem. Soc., Perkin Trans. 1*, 1984, 2641.

19 N. M. Rateb, Synthesis of Some New Thiazole, Thiophene, and 2,3-Dihydro-1,3,4-thiadiazole and Pyrimidino[1,2-b] indazole Derivatives, *Phosphorus, Sulfur, Silicon Relat. Elem.*, 2005, **180**, 2361–2372.

20 D. L. Rector, S. D. Folz, R. D. Conklin, L. H. Nowakowski and G. Kaugars, Structure-activity relationships in a broad-spectrum anthelmintic series. Acid chloride phenylhydrazones. I. Aryl substitutions and chloride variations, *J. Med. Chem.*, 2002, **24**, 532–538.

21 A. F. Hegarty, M. P. Cashman and F. L. Scott, Synthesis of aliphatic hydrazonyl bromides and kinetics of their conversion into hydrazides, *J. Chem. Soc., Perkin Trans. 2*, 1972, 1381.

22 J. Daunis, H. Lopez and G. Maury, Heteroaromatic 10-.pi.-electron systems. New s-triazolo-as-triazines with a bridgehead nitrogen atom, *J. Org. Chem.*, 2002, **42**, 1018–1022.

23 M. Tisler and Z. Vrbaski, Reaction of 4-Arylthiosemicarbazides with Some α-Keto Acids and Synthesis of Some Substituted 3-Thioxo-5-oxo-2,3,4,5-tetrahydro-1,2,4-triazines, *J. Org. Chem.*, 2002, **25**, 770–773.

24 F. M. Sroor, A. F. El-Sayed and K. Mahmoud, Novel 5-Fluorouracil analogues versus perfluorophenyl ureas as potent anti-breast cancer agents: design, robust synthesis, in vitro, molecular docking, pharmacokinetics ADMET analysis and dynamic simulations, *Bioorg. Chem.*, 2024, **153**, 107944.

25 F. M. Sroor, W. M. Basyouni, W. M. Tohamy, T. H. Abdelhafez and M. K. El-awady, Novel pyrrolo[2,3-d] pyrimidine derivatives: Design, synthesis, structure elucidation and *in vitro* anti-BVDV activity, *Tetrahedron*, 2019, **75**, 130749.

26 F. M. Sroor, A. M. Othman, K. Mahmoud and K. F. Mahrous, New 2,4-diaryl-3-azabicyclo[3.3.1]nonan-9-one derivatives as antimicrobial and anti-cancer agents: Synthesis, in-vitro and SAR studies, *J. Mol. Struct.*, 2023, **1294**, 136516.

27 F. M. Sroor, H. K. A. Elhakim, S. M. Abdelrehim, K. F. Mahrous, A. F. El-Sayed and I. A. Abdelhamid, New cyano-acrylamide derivatives incorporating the thiophene moiety: Synthesis, anti-cancer, gene expression, DNA fragmentation, DNA damage, and *in silico* studies, *J. Mol. Struct.*, 2025, **1321**, 140001.

28 A. F. Brito, A. M. Abrantes, C. Pinto-Costa, A. R. Gomes, A. C. Mamede, J. Casalta-Lopes, A. C. Gonçalves, A. B. Sarmento-Ribeiro, J. G. Tralhão and M. F. Botelho, Hepatocellular Carcinoma and Chemotherapy: The Role of p53, *Chemotherapy*, 2012, **58**, 381–386.

29 N. Yasser, F. M. Sroor, H. M. El-Shorbagy, S. M. Eissa, H. M. Hassaneen and I. A. Abdelhamid, Synthesis, anticancer evaluation of novel hybrid pyrazole-based chalcones, molecular docking, DNA fragmentation, and gene expression: *in vitro* studies, *RSC Adv.*, 2024, **14**, 21859–21873.

30 F. M. Sroor, A. A. F. Soliman, E. M. Youssef, M. Abdelraof and A. F. El-Sayed, Green, facile synthesis and evaluation of unsymmetrical carbamide derivatives as antimicrobial and anticancer agents with mechanistic insights, *Sci. Rep.*, 2024, **14**, 15441.

31 M. G. Kamel, F. M. Sroor, M. K. H. Hanafy, K. F. Mahrous and H. M. Hassaneen, Design, synthesis and potent anti-pancreatic cancer activity of new pyrazole derivatives bearing chalcone, thiazole and thiadiazole moieties: gene

expression, DNA fragmentation, cell cycle arrest and SAR, *RSC Adv.*, 2024, **14**, 26954–26970.
32 P. L. Olive, J. P. Banáth and R. E. Durand, Heterogeneity in Radiation-Induced DNA Damage and Repair in Tumor and Normal Cells Measured Using the "Comet" Assay, *Radiat. Res.*, 2012, **178**, AV35–AV42.
33 A. Collins, M. Dusinska, M. Franklin, M. Somorovska, H. Petrovska, S. Duthie, L. Fillion, M. Panayiotidis, K. Raslova and N. Vaughan, Comet assay in human biomonitoring studies: Reliability, validation, and applications, *Environ. Mol. Mutagen.*, 1997, **30**, 139–146.
34 A. Yawata, M. Adachi, H. Okuda, Y. Naishiro, T. Takamura, M. Hareyama, S. Takayama, J. C. Reed and K. Imai, Prolonged cell survival enhances peritoneal dissemination of gastric cancer cells, *Oncogene*, 1998, **16**, 2681–2686.
35 R. K. Gibb, D. D. Taylor, T. Wan, D. M. O'Connor, D. L. Doering and Ç. Gerçel-Taylor, Apoptosis as a Measure of Chemosensitivity to Cisplatin and Taxol Therapy in Ovarian Cancer Cell Lines, *Gynecol. Oncol.*, 1997, **65**, 13–22.
36 SAS Institute, *SAS User's Guide: Statistics*, SAS Institute, Cary, N.C., 1982.
37 O. Trott and A. J. Olson, AutoDock Vina: Improving the speed and accuracy of docking with a new scoring function, efficient optimization, and multithreading, *J. Comput. Chem.*, 2009, **31**, 455–461.
38 F. M. Sroor, A. F. El-Sayed and M. Abdelraof, Design, synthesis, structure elucidation, antimicrobial, molecular docking, and SAR studies of novel urea derivatives bearing tricyclic aromatic hydrocarbon rings, *Arch. Pharm.*, 2024, **357**, 2300738.
39 **https://www.rcsb.org/structure/7T7J**.
40 **https://www.rcsb.org/structure/2g76**.
41 E. W. Bell and Y. Zhang, DockRMSD: an open-source tool for atom mapping and RMSD calculation of symmetric molecules through graph isomorphism, *J. Cheminf.*, 2019, **11**, 40.
42 G. M. Sheldrick, A short history ofSHELX, *Acta Crystallogr., Sect. A:Found. Adv.*, 2007, **64**, 112–122.
43 P. W. Betteridge, J. R. Carruthers, R. I. Cooper, K. Prout and D. J. Watkin, CRYSTALSversion 12: software for guided crystal structure analysis, *J. Appl. Crystallogr.*, 2003, **36**, 1487.
44 D. S. Moss, International tables for X-ray crystallography. Vol. IV edited by J. A. Ibers and W. C. Hamilton, *Acta Crystallogr.*, 1975, **31**, 2558.
45 L. J. Farrugia, ORTEP-3 for Windows - a version ofORTEP-III with a Graphical User Interface (GUI), *J. Appl. Crystallogr.*, 1997, **30**, 565.